6-19-2015

Procollagen C-endopeptidase Enhancer Protein 2 (PCPE2) Reduces Atherosclerosis in Mice by Enhancing Scavenger Receptor Class B1 (SR-BI)-Mediated High-Density Lipoprotein (HDL)-Cholesteryl Ester Uptake

Ricquita D. Pollard
Wake Forest University

Christopher N. Blesso
University of Connecticut

Manal Zabalawi
Wake Forest University

Brian Fulp
Wake Forest University

Mark Gerelus
Wake Forest University

See next page for additional authors

Authors
Ricquita D. Pollard, Christopher N. Blesso, Manal Zabalawi, Brian Fulp, Mark Gerelus, Xuewei Zhu, Erica W. Lyons, Nebil Nuradin, Omar L. Francone, Xiang-An Li, Daisy Sahoo, Michael J. Thomas, and Mary G. Sorci-Thomas

Procollagen C-endopeptidase Enhancer Protein 2 (PCPE2) Reduces Atherosclerosis in Mice by Enhancing Scavenger Receptor Class B1 (SR-BI)-Mediated High-Density Lipoprotein (HDL)-Cholesteryl Ester Uptake

Notes/Citation Information
Published in *The Journal of Biological Chemistry*, v. 290, no. 25, p. 15496-15511.

Digital Object Identifier (DOI)
https://doi.org/10.1074/jbc.M115.646240

THE JOURNAL OF BIOLOGICAL CHEMISTRY VOL. 290, NO. 25, pp. 15496–15511, June 19, 2015

Procollagen C-endopeptidase Enhancer Protein 2 (PCPE2) Reduces Atherosclerosis in Mice by Enhancing Scavenger Receptor Class B1 (SR-BI)-mediated High-density Lipoprotein (HDL)-Cholesteryl Ester Uptake*

Received for publication, February 17, 2015, and in revised form, April 7, 2015 Published, JBC Papers in Press, May 6, 2015, DOI 10.1074/jbc.M115.646240

Ricquita D. Pollard[‡1], Christopher N. Blesso[§2], Manal Zabalawi[‡], Brian Fulp[‡], Mark Gerelus[‡], Xuewei Zhu[‡], Erica W. Lyons[‡], Nebil Nuradin[¶], Omar L. Francone[‖], Xiang-An Li[**], Daisy Sahoo[¶3], Michael J. Thomas[¶], and Mary G. Sorci-Thomas[¶4]

*From the [¶]Department of Medicine and the Department of Pharmacology and Toxicology, Medical College of Wisconsin, Milwaukee, Wisconsin 53226, the [‡]Section of Molecular Medicine, Department of Internal Medicine and the Department of Biochemistry, Wake Forest University School of Medicine, Winston-Salem, North Carolina 27101, the [§]Department of Nutritional Sciences, University of Connecticut, Storrs, Connecticut 06268, [‖]Shire Human Genetic Therapies, Lexington, Massachusetts 02421, and the **Department of Pediatrics, University of Kentucky, Lexington, Kentucky 40506*

Background: Extracellular matrix protein PCPE2 is linked to alterations in HDL size and concentration.
Results: PCPE2 protects against diet-induced atherosclerosis by promoting HDL catabolism, reverse cholesterol transport, and SR-BI-mediated uptake of HDL-cholesteryl ester.
Conclusion: PCPE2 mediates HDL function by reducing lipid and immune cell accumulation in the artery.
Significance: These findings establish a role for the extracellular matrix glycoprotein PCPE2 in SR-BI-mediated HDL function and the prevention of atherosclerosis.

Studies in human populations have shown a significant correlation between procollagen C-endopeptidase enhancer protein 2 (PCPE2) single nucleotide polymorphisms and plasma HDL cholesterol concentrations. PCPE2, a 52-kDa glycoprotein located in the extracellular matrix, enhances the cleavage of C-terminal procollagen by bone morphogenetic protein 1 (BMP1). Our studies here focused on investigating the basis for the elevated concentration of enlarged plasma HDL in PCPE2-deficient mice to determine whether they protected against diet-induced atherosclerosis. PCPE2-deficient mice were crossed with LDL receptor-deficient mice to obtain $LDLr^{-/-}$, $PCPE2^{-/-}$ mice, which had elevated HDL levels compared with $LDLr^{-/-}$ mice with similar LDL concentrations. We found that $LDLr^{-/-}$, $PCPE2^{-/-}$ mice had significantly more neutral lipid and CD68+ infiltration in the aortic root than $LDLr^{-/-}$ mice. Surprisingly, in light of their elevated HDL levels, the extent of aortic lipid deposition in $LDLr^{-/-}$, $PCPE2^{-/-}$ mice was similar to that reported for $LDLr^{-/-}$, apoA-$I^{-/-}$ mice, which lack any apoA-I/HDL. Furthermore, $LDLr^{-/-}$, $PCPE2^{-/-}$ mice had reduced HDL apoA-I fractional clearance and macrophage to fecal reverse cholesterol transport rates compared with $LDLr^{-/-}$ mice, despite a 2-fold increase in liver SR-BI expression. PCPE2 was shown to enhance SR-BI function by increasing the rate of HDL-associated cholesteryl ester uptake, possibly by optimizing SR-BI localization and/or conformation. We conclude that PCPE2 is atheroprotective and an important component of the reverse cholesterol transport HDL system.

In humans there is an inverse correlation between the concentration of plasma HDL and the relative risk of developing cardiovascular disease (CVD)[5] (1–4). To explain this association, many studies have suggested that HDL plays a central role in the pathway called reverse cholesterol transport (RCT), a process that returns cholesterol to the liver for excretion (5, 6). In the first step, ATP-binding cassette transporter A1 (ABCA1) lipidates apoA-I with phospholipid and cholesterol to form nascent HDL (nHDL) (5, 7–9). These nHDL are rapidly converted to mature HDL by plasma lecithin-cholesterol acyltransferase, an enzyme that esterifies free cholesterol yielding mature spherical HDL particles with a cholesteryl ester (CE)-rich core. The RCT pathway is complete when the scavenger receptor class B1 (SR-BI) in the liver removes CE from mature HDL, leaving lipid-poor apoA-I to be recycled or filtered by the kidney (10). Because the liver is the primary site of HDL metabo-

* This work was supported, in whole or in part, by National Institutes of Health Grants NHLBI HL-112270, HL 112276, and HL 127649 (to M. G. S.-T.). This work was also supported by American Heart Association Grants 09GRNT2280053 and 14GRNT20500029 (to M. J. T.). The authors declare that they have no conflicts of interest with the contents of this article.
[1] Supported by National Institutes of Health Diversity Supplement Grant HL112270A1S1.
[2] Supported by post-doctoral American Heart Association Grant 13POST17000005.
[3] Supported by National Institutes of Health Grant RO1-HL058012.
[4] To whom correspondence should be addressed: Dept. of Medicine, Div. of Endocrinology, Metabolism, and Clinical Nutrition, Medical College of Wisconsin, 8701 W. Watertown Plank Rd., Milwaukee, WI 53226. Tel.: 414-955-5728; Fax: 414-456-6312; E-mail: msthomas@mcw.edu.

[5] The abbreviations used are: CVD, cardiovascular disease; RCT, reverse cholesterol transport; ABCA1, ATP-binding cassette transporter A1; nHDL, nascent HDL; CE, cholesteryl ester; SR-BI, scavenger receptor class B1; PCPE2, procollagen C-endopeptidase enhancer protein 2; BMP1, bone morphogenetic protein 1; NTR, netrin-like; OCT, optimal cutting temperature (medium); ^{3}H-COE, cholesteryl [1a,2a-^{3}H]oleoyl ether; FCR, fractional catabolic rate.

lism, the steady-state concentration of plasma HDL depends largely on the rate of nHDL formation balanced by the catabolism of HDL.

For some time, epidemiology studies used plasma HDL concentration to help calculate the relative risk of developing CVD. That approach has been criticized because plasma HDL concentration does not adequately predict an individual's CVD risk (11, 12). Recent studies have shown that an individual's cholesterol efflux capacity is a more accurate measure of assessing CVD risk (13–15). Efflux capacity measures the potential of an individual's apoB-depleted plasma to mobilize cellular cholesterol, suggesting that the inherent properties of one's plasma HDL are responsible for driving this process.

Cholesterol efflux is an essential physiological process that produces nHDL particles. It is now recognized that the composition and structure of nHDL, before modification in plasma, differ significantly from plasma or mature HDL. These nHDL particles contain three apoA-I monomers and are highly enriched in free cholesterol and sphingomyelin, having a composition similar to lipid rafts (16).

nHDL formation is not a spontaneous process occurring when apoA-I and phospholipid come in contact. Rather, nHDL formation requires carefully orchestrated conformational changes in the apoprotein structure that permit shielded, hydrophobic residues within multiple monomers of apoA-I to become accessible and bind phospholipid (16). This process yields ~11-nm diameter nHDL particles carrying over 100 molecules of free cholesterol/particle (17), an efficient process to efflux cholesterol from the cell.

Several mechanisms have been proposed to explain how nHDL is assembled via ABCA1 on the membrane surface (7, 18, 19). One hypothesis has binding of lipid-poor apoA-I to ABCA1 as the first step in the process. However, other studies suggest that low affinity, high capacity membrane binding sites are involved before apoA-I binds to ABCA1 (20–23). Interaction between apoA-I and membrane-bound accessory protein(s) could potentially promote conformational changes within lipid-poor apoA-I and in so doing enhance the rate of nHDL particle formation (12, 24, 25).

Recent reports suggest that procollagen C-endopeptidase enhancer protein 2 (PCPE2) participates in promoting cholesterol efflux. A connection between PCPE2 and HDL was inferred when significant correlations were observed between PCPE2 single nucleotide polymorphisms and plasma HDL cholesterol concentrations (26). PCPE2 is a 52-kDa glycoprotein encoded by the *PCOLCE2* gene (27, 28). It shares 43% amino acid sequence identity with PCPE1 (29). Both PCPE1 and PCPE2 are located in the extracellular matrix, where they facilitate bone morphogenetic protein 1 (BMP1) cleavage of C-terminal procollagen propeptides. PCPE2 and PCPE1 have different tissue distributions and heparin-binding affinities, suggesting a functional divergence (29). PCPE2 is heavily expressed in heart tissue in contrast to PCPE1. Both PCPE1 and PCPE2 have two CUB (Complement C1r/C1s, Uegf, Bmp1) domains separated by a short linker region (30–32), with each domain consisting of about 110 residues containing a β-sandwich fold that mediates a variety of protein-protein interactions. The CUB domains also contain a homologous Ca^{2+} binding site that mediates ionic interactions between protein partners, similar to that described in the low-density lipoprotein receptor family (33). The tandem CUB domains are followed by a C-terminal netrin-like (NTR) domain (27, 29). CUB domains are commonly found in extracellular membrane proteins that mediate protein-protein interactions (33–36), whereas NTR domains bind to cell surface glycosaminoglycans (37, 38), presumably anchoring PCPE2 to the extracellular matrix.

Interestingly, BMP1, in addition to catalyzing procollagen processing, removes the apoA-I six-amino acid propeptide (39). Studies by Francone and others (26, 40, 41) show that PCPE2 stabilizes a ternary catalytic complex with apoA-I and BMP1. These findings suggest that BMP1-PCPE2 processing of the apoA-I propeptide might stimulate nHDL assembly (42).

Studies in $PCPE2^{-}$-deficient mice provide the first direct experimental evidence linking PCPE2 to HDL metabolism (43). PCPE2 knock-out mice had elevated concentrations of enlarged plasma HDL (44), despite displaying defective ABCA1-mediated cholesterol efflux capacity. Thus, reduced cholesterol efflux is paradoxically associated with elevated plasma HDL cholesterol in PCPE2-deficient mice. A recent genome-wide siRNA screen also suggests that PCPE2 affects the efficiency of HDL apoA-I secretion (45).

Because elevated plasma HDL levels are associated with reduced atherosclerosis, we sought to investigate whether elevated concentrations of enlarged HDL in PCPE2-deficient mice were atheroprotective or atherogenic. We have suggested mechanisms to explain the role of PCPE2 and provided evidence demonstrating the participation of PCPE2 in HDL cholesterol catabolism and reverse cholesterol transport.

Experimental Procedures

Animals and Diets—PCPE2-deficient mice in the C57BL/6 background were obtained from the Max Planck Institute (43) and then crossed with $LDLr^{-/-}$ mice to generate $LDLr^{-/-}$, $PCPE2^{-/-}$ mice. Both $LDLr^{-/-}$ and $LDLr^{-/-}$, apoA-$I^{-/-}$ mice have been fully crossed onto the C57BL/6 background as described previously (46, 47). Starting at 6 weeks of age, mice were fed for 12 weeks either a standard chow diet or an atherogenic diet containing 0.1% cholesterol and 10% calories from palm oil (47). Mice were fasted for 3 h prior to being anesthetized with ketamine/xylazine (200 mg/kg ketamine and 10 mg/kg xylazine) followed by euthanasia and blood collection by cardiac puncture. The Animal Care and Use Committee of the Wake Forest University School of Medicine approved all procedures used in the current study. All mice were housed in a temperature-controlled room and maintained in a 12-h light/12-h dark cycle at the Wake Forest School of Medicine vivarium.

Plasma Lipoprotein Isolation and Characterization—Blood was collected in EDTA containing tubes then centrifuged at 15 °C for 10 min at 7000 rpm. The plasma fraction was collected and stored at −80 °C. Total plasma cholesterol (Wako Diagnostics Cholesterol E) was determined using an enzymatic assay kit. For total lipoprotein cholesterol distribution, 15 μg of total plasma cholesterol was applied to a Superose 6 10/300GL column (GE Healthcare) with online mixing of enzymatic reagent

(Cholesterol (Liquid) Reagents Set, Pointe Scientific Inc.) as described previously (48). Isolation of the total lipoprotein fraction for compositional analysis was carried out by first obtaining the $d < 1.225$ g/ml fraction after density gradient ultracentrifugation using KBr as described previously (46). The $d < 1.225$ g/ml fractions were separated into lipoprotein classes using size-exclusion fast protein liquid chromatography (FPLC) (46). Aliquots corresponding to VLDL, LDL, and HDL classes were pooled and stored at −80 °C for composition analysis or used immediately for particle size determination. The HDL particle size was determined by a comparison with standards of known Stokes diameter following separation using Novex (Life Technologies) 4–20% non-denaturing gels and then stained with Coomassie Blue G-250 dye as described previously (49). Mouse plasma apoA-I concentration was measured using an enzyme-linked immunosorbent assay as described previously (49).

Quantification of Pro-apolipoprotein A-I by Mass Spectrometry—The abundance of pro-apoA-I and apoA-I was assessed from purified HDL and whole plasma from PCPE2$^{-/-}$ and C57BL/6 mice using liquid chromatography-tandem mass spectrometry. Whole plasma aliquots were separated on 12% SDS-PAGE as described previously (16, 50–52). The gel was stained with SimplyBlue (Life Technologies), and the protein band corresponding to 28,000 Da was excised from the gel, minced, and repeatedly dehydrated with acetonitrile. The gel pieces were rehydrated with a cold, freshly prepared solution containing 20 ng/μl trypsin in 10 mM ammonium bicarbonate, pH 7.8, 0.1% (w/v) RapiGest SF^{TM}, and 1 mM $CaCl_2$. The final trypsin to apoA-I mass ratio was ~1:20. After incubation on ice for 10 min, the digests were incubated for 18 h at 37 °C. The digestion solution was removed, and gel pieces were covered with 200 μl of acetonitrile/formic acid/water (v/v/v, 50:5:45). After sitting for 10 min the solvent was transferred to a fresh tube. The extraction was repeated and the combined aliquots acidified to an HCl:apoA-I ratio of 1:10 (v/v) using 500 mM HCl. After the acidified solution was incubated for 35 min at 37 °C, the sample was centrifuged for 10 min at 13,000 rpm. The supernatant was transferred to a fresh tube before mass spectrometry. Survey scans were performed on each peptide mixture using a Waters Q-TOF API-US mass spectrometer equipped with a Waters CapLC and Advion Nanomate source. Acquisition was controlled using Mass-Lynx^{TM} 4.0 software. Peptides were loaded onto a PLRP-S trapping column, 0.5-mm diameter × 2.0-mm length, containing 3-μm diameter particles with a pore diameter of 100 Å. Peptides were loaded onto the trapping column in water/acetonitrile/formic acid (97:3:0.2) at 500 nl/min. After switching of the trapping column, in-line separation was accomplished on a 0.3 × 150-mm PCRP-S column packed with 3-μm diameter particles with 100 Å pores at 470 nl/min. The following gradient elution was used: solvent A (25 mM formic acid in 97% water and 3% acetonitrile) and solvent B solvent B (25 mM formic acid in 3% water 97% acetonitrile). The gradient profile was: 2% solvent B for 3 min with a linear increase to 40% B at 90 min and then to 80% B in 5 min. At 95 min, the composition was ramped to 2% B over 5 min and equilibrated with 2% B for 30 min. Positive ion survey scans were recorded in the continuum mode with a scan window of 300 to 1500 m/z for 2 s. The source temperature was 80 °C and cone voltage was 45 V. Experimental m/z was corrected using mouse apoA-I tryptic fragment 7, $m/z = 533.7462$. Ions within ±0.051 m/z of the theoretical ions were sequenced. Product ion MS/MS spectra were acquired in the continuum mode from 50 to 1500 m/z using a data-directed charge state-selective collision energy and an accumulation time of 2 s. Sequence analysis of the MS/MS spectra was performed with a fragment ion tolerance of ±0.05 m/z.

For quantification of the ratio of mature and pro-apoA-I, the N-terminal tryptic peptides for mouse pro-apoA-I (WHVWQQDEPQSQWDK, protonated $m/z = 1996.8942$) and mature mouse apoA-I (DEPQSQWDK, protonated $m/z = 1132.4911$) were synthesized (GenScript), and the m/z, purity, and sequence were verified by mass spectrometry. The retention time, mass, and sequence were used to identify the N-terminal sequence from all samples analyzed.

For the analysis of intact pro- or mature mouse apoA-I from purified HDL, mass spectrometric analysis was performed using a Waters Q-TOF equipped with an Advion Triversa Nanomate source as described previously (53). Samples (0.4 μM) were prepared in 1:1 (v:v) acetonitrile-water containing 0.2% formic acid and then introduced into the mass spectrometer at 500 nl/min. Acquisition parameters were adjusted to maximize resolution.

Lipid Composition—Total and free cholesterol determination were performed on aliquots from FPLC-separated and pooled HDL that had been spiked with the internal standard, cholesterol-3,4-$^{13}C_2$ (Sigma-Aldrich), and subjected to lipid extraction as previously described (16). To measure free cholesterol an aliquot was removed, evaporated under argon, dissolved in hexane and then injected on a Finnigan TSQ Quantum XLS tandem mass spectrometer interfaced to a TRACE gas chromatograph (GC-MS/MS), as described previously (16, 47), by select reaction monitoring (SRM) with the following parameters in the positive ion mode: scan time, 0.1 s; collision energy, 10 V; emission current, 25 μA; electron energy, −42 eV; source and transfer line temperature, 260 °C; and flow rate, 1 ml/min. Analysis was carried out using a DB-1 column (10.4 m, 250 μm inner diameter) with a 0.25-μM film thickness. For quantifying total cholesterol, the remaining sample was dried under a stream of nitrogen, redissolved in 1 ml of ethanol, mixed with 100 μl of 50% (w/w) aqueous potassium hydroxide, and then saponified for 1 h at 60 °C. After extraction, total cholesterol was measured on the Quantum XLS. Cholesteryl ester was calculated as the difference between free cholesterol and total cholesterol.

Plasma triglycerides were analyzed using mass spectrometry from mouse plasma after preliminary separation from other polar and nonpolar lipids using aminopropyl solid-phase extraction columns using the procedure of Kaluzny *et al.* (54) with minor modifications. The nonpolar fraction was dried under nitrogen and loaded onto the second solid-phase extraction column dissolved in 500 μl of hexane. Cholesteryl esters were removed from the column with 3–4-ml washes of 4% CH_2Cl_2 in hexane. Then triglycerides were eluted with 3–8-ml washes of CH_2Cl_2:diethyl ether:hexane (14:1:84). Quantitation was by gas chromatography-mass spectrometry after saponifi-

cation to generate methylated fatty acids (55, 56). The fatty acids were quantified to obtain the total fatty acid composition. The moles of fatty acids were summed and divided by 3 to obtain the number of moles of triglyceride. C17 triglyceride was used as the internal standard.

RNA Isolation, cDNA Synthesis, and Quantitative Real-Time-PCR—Tissues harvested at necropsy were flash-frozen with liquid nitrogen and kept at −80 °C until needed. Briefly, tissue was quickly thawed, weighed, and then added to a 14-ml screw cap polypropylene tube containing 1 ml of pre-chilled TRIzol (Life Technologies). The tissue was immediately homogenized using a Polytron PT 1200C homogenizer, and RNA was isolated following the manufacturer's instructions. Purified RNA pellets were thoroughly resuspended in Ultra-Pure water (Sigma-Aldrich) on ice. RNA concentrations were determined at 260 nm using a Beckman DU800 spectrophotometer.

Using 1–2 μg of RNA, cDNA was synthesized using the qScript cDNA Supermix (Quant BioSciences) according to the manufacturer's instructions. Quantitative real-time PCR was performed using the Applied Biosystems 7500 Fast Real Time PCR system with Fast Start Universal SYBR Green Master Mix (Roche Applied Science) according to the manufacturer's instructions. Reactions were set up in triplicate using a 1-μg/μl cDNA template. Following amplification, Ct values were obtained from Applied Biosystems sequence detection software, and the ΔCt values were determined for the gene of interest compared with that for mouse GAPDH for each animal run as a control. For each tissue the percent relative abundance of mouse PCPE2 and PCPE1 was derived from the $\Delta Ct_{max} - \Delta Ct/\Delta Ct_{max}) \times 100$. Primers designed using the Universal Probe Library were purchased from Integrated DNA Technologies. The following are the mouse sequences used: SR-BI forward, GCCCATCATCATCTGCCAACT, and reverse, TCCTGGGAGCCCTTTTTACT; PCPE1 forward, TTACGTGGCAAGTGAGGGTTT, and reverse, TGTCCAGATGCACTTCTTGTTTG; and PCPE2 forward, TCACATGTGGCGGCATTCT, and reverse, CAGGAAAACCTTCACTGCCAAT.

Immunoblotting—Immunoblotting was performed subsequent to total tissue protein isolation following extraction using a radioimmune precipitation assay buffer (RIPA, Cell Signaling Technologies) or using detergent-free lipid raft isolation as described. For tissues extracted with radioimmune precipitation assay buffer, aliquots of equal protein content were run on 12% SDS-PAGE. All sample aliquots were diluted with 4× LDS buffer (Novex) to which solid DTT had been added to achieve a 100 mM final concentration. Samples were heated to 70 °C for 10 min. Transfer to PVDF membrane (PerkinElmer Life Sciences) was accomplished after treatment with Tris-glycine, pH 8.3, buffer using a semi-dry blot (Bio-Rad) apparatus for 30 min at 10 V. Membranes were blocked with 5% nonfat dry milk in 10 mM Tris-glycine, pH 7.4, buffer and processed. The primary antibodies used (PCPE1 (Novus Biologicals), PCPE2 (Abcam), GAPDH (Ambion), and SR-BI (Novus Biologicals)) were diluted 1:1000 and incubated with the membrane at 4 °C overnight. The blots were washed and then incubated with an HRP-conjugated anti-mouse IgG secondary antibody (GE Healthcare) at a 1:10,000 dilution for 1 h at room temperature. Blots were washed again and then incubated with SuperSignal West Pico chemiluminescence substrate (Pierce) and visualized with a FujiFilm LAS-3000 camera. Band intensities were compared using MultiGauge software (FujiFilm).

HDL ApoA-I Turnover—Diet-fed mouse HDL was purified using a combination of ultracentrifugation and FPLC. The purified HDL apoA-I was then labeled with ^{125}I using the McFarlane method (57) as described previously (58, 59). Sufficient ICl was used to have 0.5 mol of radiolabeled iodine for every mole of HDL apoA-I and prevent damage to the protein or labeling lipid. Labeled HDL apoA-I was purified from free iodine using a desalting column (Bio-Rad), and the eluate was dialyzed exhaustively against 0.15 M NaCl, pH 7.4. On the day of the study, anesthetized mice were retro-orbitally injected with ^{125}I-radiolabeled HDL (10×10^6 cpm) after isoflurane administration. Approximately 30 μl of blood was collected from the contralateral retro-orbital sinus at 0.08, 0.17, 0.5, 1, 3, 6, 22, 28, and 48 h. Radioactivity was measured at each time point using a Beckman Gamma 4000 counter. The fractional catabolic rates and half-lives of the ^{125}I-labeled HDL were determined from plasma decay curves assuming a one-pool model (58). Blood volumes were estimated to be 5.85 ml/100 g of body weight.

Histology and Immunofluorescence Microscopy—At the time of sacrifice, a 21-gauge butterfly needle was inserted into the left ventricle; the atrium was clipped, and the heart and aorta were perfused with saline for 5 min and then removed and cleaned of fat and adventitia. Mouse heart and aorta were embedded in optimal cutting temperature (OCT) medium and then sectioned for staining and immunohistochemistry. For quantification of total and percent lesion area, OCT-embedded aortas were cut into sequential 6-μm sections using a Leica cryostat at −50 °C. Tissue sections were stained overnight in 0.5% Oil Red O dissolved in propylene glycol and then counterstained with hemotoxylin. Masson's trichrome stain was used to assess the connective tissue content of the aortic root. Sections were digitized using a Nikon microscope and Image-Pro Plus 6.2 software and then quantified using NIS-Elements software (Nikon Instruments Inc.). Eight to 10 sections at intervals of 30 μm were used for morphological analyses and were averaged to obtain a value for each animal. The results are expressed as both the percentage of lesion area and absolute lesion area.

For immunofluorescence microscopy, purified rat anti-mouse CD68 (AbD FA-11-Serotec) at a 1:100 dilution was used as the primary antibody. Slides were incubated for 1 h in PBS buffer containing 2% fetal calf plasma, washed with PBS, and then incubated with a 1:300 dilution of Cy3-conjugated goat anti-rat IgG antibody (Rockland) for 30 min at room temperature. After the slides were washed briefly with PBS, they were stained with DAPI to visualize the nuclei and then mounted with Fluoro-Gel (Electron Microscopy Sciences). Immunofluorescence was visualized using a Nikon Eclipse TE2000-S microscope, and the total and percentage of CD68 staining was quantified using NIS-Elements software.

Picrosirius red staining of mouse tissues was performed on formalin-fixed tissue embedded in paraffin and then cut serially in 6-μm sections. Collagen fibers were stained using picrosirius red (Polysciences Inc.) and viewed with polarized light as described (60).

In Vivo Reverse Cholesterol Transport Studies—Diet-fed mice received an intraperitoneal injection of 0.6×10^6 dpm of [^{3}H]cholesterol-labeled J774 cells as described previously (61). Blood was collected at 6, 24, and 48 h, and the plasma was counted for radioactive content (62). Feces collected from 0 to 48 h and subjected to lipid extraction were then counted for radioactive content of neutral and acidic sterols as described previously (63).

Tissue Culture and Transfection—CHO cells were grown in DMEM/F-12 medium (1:1) supplemented with 10% (v/v) FBS, 100 units/ml penicillin, 100 μg/ml streptomycin, and 2 mM L-glutamine. Transient transfections were performed using Lipofectamine 2000 according to the manufacturer's protocol (Life Technologies) with 2.5 μg of DNA and 12 μl of Lipofectamine 2000/well of a confluent 6-well plate. The human PCPE2-pCMV6 plasmid used in the transfection was obtained from OriGene (Rockville, MD) and contains a Myc-DDK tag at the N terminus, which adds 10 amino acids.

Selective Uptake of HDL Labeled with [^{3}H]Cholesteryl Oleyl Ether—HDL isolated as described above, using a combination of ultracentrifugation and FPLC, was labeled with cholesteryl [1a,2a-^{3}H]oleoyl ether (^{3}H-COE) (American Radiolabeled Chemicals Inc.) using recombinant cholesterol ester transfer protein (CETP, Roar Biomedical Inc.) as described (64). An aliquot containing 10 μg of labeled HDL (based on protein)/ml of plasma-free DMEM medium plus 0.5% BSA was incubated with confluent CHO cells in a 6-well plate at 37 °C for 1.5 h. After incubation the medium was removed, and the cells were washed extensively to remove surface-bound labeled HDL. The cell monolayer was lysed with 1 ml of 0.1 N NaOH, and aliquots of the lysed cells were counted for their ^{3}H radioactivity content and normalized to total cell protein as determined by the Lowry assay (65).

Surface Staining of CHO Cells—Transfected CHO cells were harvested from 6-well plates and stained for SR-BI and PCPE2 using fluorescence-activated cell sorting (FACS) as described previously (66). Briefly, 3×10^5 cells were stained with polyclonal rabbit anti-SR-BI-APC conjugate (Alexa Fluor 647) (Bioss Antibodies) and mouse anti-MycDDK-FITC conjugate (Alexa Fluor 488) (AbD Serotec) for 30 min at 4 °C. Samples were washed and resuspended in 2% paraformaldehyde in PBS before acquisition of samples using a system (BD Biosciences).

Statistical Analysis—GraphPad Prism version 5 was used for statistical analysis, and the data are reported as mean ± S.D. Differences between groups were evaluated by independent *t* tests and by analysis of variance with Tukey's post hoc test.

Results

The Absence of PCPE2 Affects Lipoprotein Distribution and Concentration—PCPE2-deficient mice in the C57BL/6 background (43) were characterized with respect to HDL size and concentration for comparison with the previously published phenotype (44). Fig. 1*A* shows the cholesterol distribution following FPLC separation of the major lipoprotein classes from the $d < 1.225$ g/ml density fraction. We see that PCPE2-deficient mice possess a greater concentration of enlarged HDL particles (Fig. 1*A*, *dashed line*) compared with control C57BL/6 mice that express PCPE2 (*solid line*). The increase in the HDL cholesterol concentration in PCPE2-deficient mice was accompanied by an elevation in plasma apoA-I concentrations as shown in Table 1. These changes in HDL levels were independent of statistically significant changes in LDL or VLDL cholesterol levels between genotypes. A trend to higher plasma triglycerides was observed for chow-fed PCPE2-deficient mice, as exemplified by the increased VLDL peak in Fig. 1*A*, but the trend was not statistically significant. Non-denaturing gradient gel separation confirmed that PCPE2$^{-/-}$ mice had larger HDL particle sizes and diameters compared with HDL from control mice, as shown in Fig. 1*B* and consistent with the previous study (44). The cholesterol to apoA-I composition was determined in HDL particles purified by a combination of density ultracentrifugation and FPLC. Fig. 1*C* shows that HDL particles from PCPE2$^{-/-}$ mice were enriched in total cholesterol when normalized to apoA-I content, likely accounting for the increase in particle size. However, HDL from both genotypes had similar ratios of esterified to total cholesterol (Fig. 1*C*, *EC*/*TC*), suggesting that plasma lecithin-cholesterol acyltransferase activity was similar for the two genotypes and that conversion of free cholesterol to esterified cholesterol was not involved in particle enlargement.

To investigate the atherosclerotic properties of PCPE2 HDL, PCPE2-deficient mice were crossed with the hypercholesterolemic LDL receptor-deficient (LDLr$^{-/-}$) mouse, to create LDLr$^{-/-}$, PCPE2$^{-/-}$ mice. Aliquots of plasma from 12 weeks chow-fed LDLr$^{-/-}$, PCPE2$^{-/-}$ mice were centrifuged to obtain the $d < 1.225$ g/ml lipoprotein fraction, which was then separated into lipoprotein classes by FPLC. Fig. 1*D* shows the lipoprotein cholesterol distribution for LDLr$^{-/-}$, PCPE2$^{-/-}$ (*dashed line*) and LDLr$^{-/-}$ mice (*solid line*). As anticipated, HDL from LDLr$^{-/-}$, PCPE2$^{-/-}$ mice contained larger sized particles, indicated by elution in earlier eluting fractions as seen in PCPE2$^{-/-}$ mouse plasma (Fig. 1*A*). The HDL cholesterol concentration in LDLr$^{-/-}$, PCPE2$^{-/-}$ mice was also significantly increased compared with LDLr$^{-/-}$ mice, as shown in Table 2.

Lipoprotein cholesterol distribution was then evaluated after feeding an atherogenic diet (46, 47, 67) for 12 weeks (results shown in Fig. 1*E*). As expected, both LDLr$^{-/-}$, PCPE2$^{-/-}$ and LDLr$^{-/-}$ mice had substantial increases in VLDL and LDL cholesterol levels. Table 2 shows a comparison of these values with their chow-fed counterparts. Interestingly, although diet-fed LDLr$^{-/-}$, PCPE2$^{-/-}$ mice did not show a significant difference in LDL cholesterol concentrations between genotypes, there was a statistically significant increase (~90%) in VLDL and HDL cholesterol concentration. These results suggest that feeding an atherogenic diet to hypercholesterolemic mice that lack PCPE2 appears to also affect VLDL in addition to HDL metabolism.

PCPE2 Protects against Diet-induced Atherosclerosis—Groups of male LDLr$^{-/-}$, PCPE2$^{-/-}$, LDLr$^{-/-}$, and LDLr$^{-/-}$, apoA-I$^{-/-}$ mice were fed an atherogenic diet. After 12 weeks of diet feeding their hearts and aortas were embedded into OCT, sectioned, and stained with Oil Red O. The extent of atherosclerotic lipid accumulation was assessed by staining aortic root sections with the neutral lipid stain followed by quantification, as shown in Fig. 2*A*. Representative Oil Red O-stained aortic

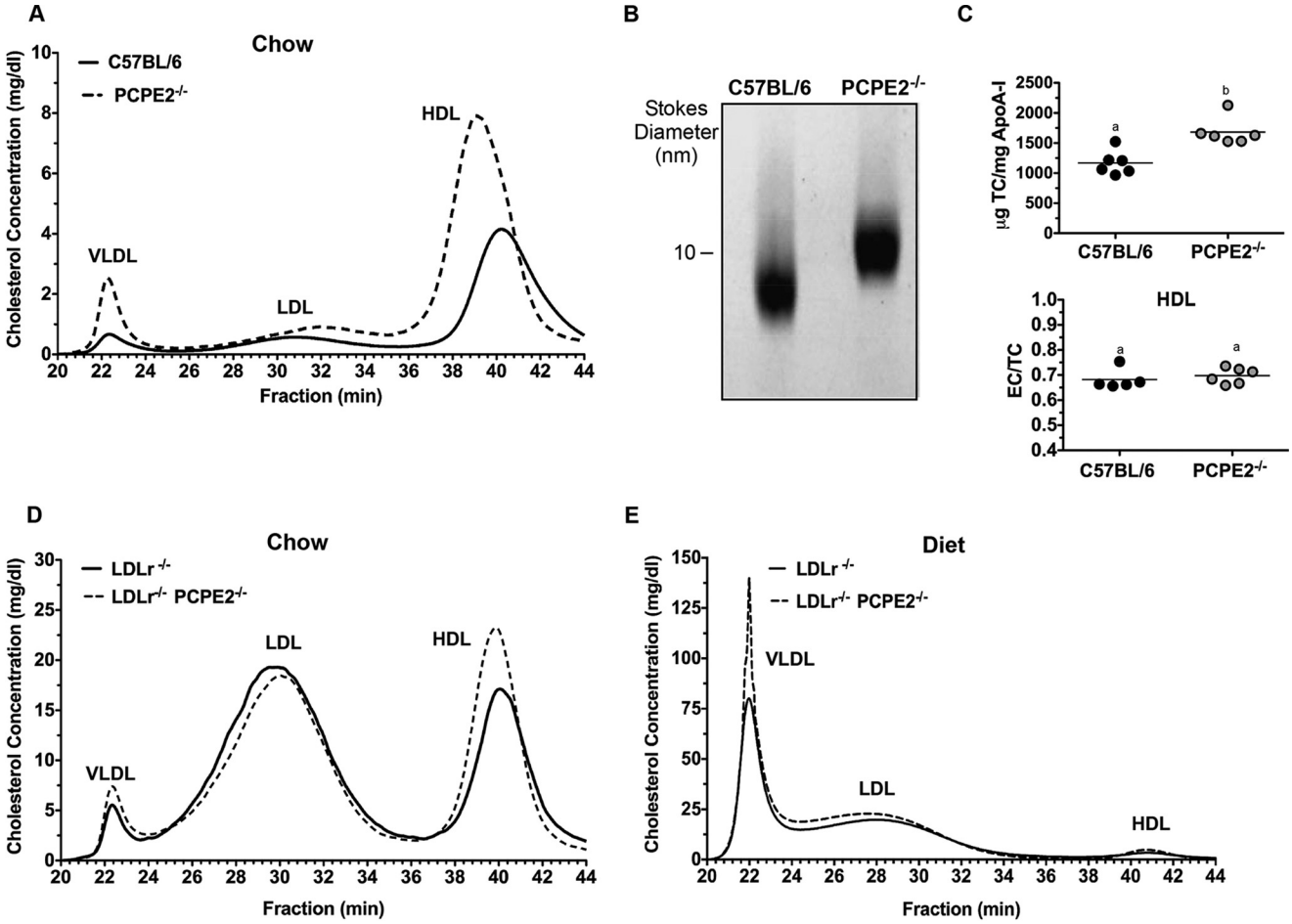

FIGURE 1. **PCPE2 deficiency alters lipoprotein cholesterol and particle size.** *A*, FPLC separation of the major lipoprotein classes expressed as cholesterol concentration from representative age- and gender-matched C57BL/6 and PCPE2$^{-/-}$ mice on a chow-fed diet. *B*, a Coomassie Blue-stained 4–20% non-denaturing gradient gel separation of a $d < 1.225$ g/ml lipoprotein fraction from chow-fed C57BL/6 and PCPE2$^{-/-}$ mice. *C*, *top*, the HDL composition as total cholesterol (*TC*) to apoA-I mass ratio for HDL after FPLC isolation for each genotype. *Bottom*, the mass ratio of esterified cholesterol (*EC*) to total cholesterol as determined by mass spectrometric analysis and an enzyme-linked immunosorbent assay as described under "Experimental Procedures." *D*, FPLC separation of the major lipoprotein classes expressed as cholesterol concentration from LDLr$^{-/-}$ and LDLr$^{-/-}$, PCPE2$^{-/-}$ mice fed a chow diet. *E*, FPLC separation of the major lipoprotein classes expressed as cholesterol concentration from 12 weeks atherogenic diet-fed LDLr$^{-/-}$ and LDLr$^{-/-}$, PCPE2$^{-/-}$ mice. Data shown are the mean of $n = 6$ male mice for each genotype condition. *Different letters* in *D* indicate statistical significance at $p < 0.05$.

TABLE 1

Plasma cholesterol and triglycerides

Fasting plasma cholesterol and triglyceride concentrations were obtained from equal numbers of male and female mice fed a chow diet for 12 weeks.

Lipoprotein/Lipid[a]	C57BL/6	PCPE2$^{-/-}$
	mg/dl	*mg/dl*
Plasma cholesterol	79 ± 14^b	121 ± 29^c
VLDL-C	3 ± 1^b	5 ± 3^b
LDL-C	14 ± 3^b	12 ± 4^b
HDL-C	55 ± 8^b	86 ± 21^c
Plasma triglycerides	69 ± 11^b	78 ± 8^b
ApoA-I	55 ± 14^b	98 ± 18^c

[a] Each lipoprotein cholesterol and apoprotein value represents the mean ± S.D. of $n = 6$ mice/genotype. Lipoproteins were purified by a combination of ultracentrifugation and FPLC. Their lipid and protein content was determined as described under "Experimental Procedures." Statistical differences at $p < 0.05$ for each row are indicated by different letters.

TABLE 2

Chow diet *versus* atherogenic diet

Fasting plasma cholesterol and fasting triglyceride concentrations were obtained from age-matched male mice fed a chow diet or an atherogenic diet for 12 weeks.

	Chow diet		Atherogenic diet	
Lipoprotein/Lipids[a]	LDLr$^{-/-}$	LDLr$^{-/-}$ PCPE2$^{-/-}$	LDLr$^{-/-}$	LDLr$^{-/-}$ PCPE2$^{-/-}$
	mg/dl	*mg/dl*	*mg/dl*	*mg/dl*
Total cholesterol	230 ± 30^b	300 ± 34^c	1248 ± 109^d	1520 ± 50^e
VLDL-C	5 ± 1^b	4 ± 2^b	448 ± 252^c	703 ± 257^d
LDL-C	92 ± 7^b	88 ± 1^b	583 ± 209^c	631 ± 126^c
HDL-C	48 ± 6^b	67 ± 8^c	52 ± 11^b	131 ± 17^d
Triglycerides	190 ± 12^b	230 ± 30^b	310 ± 57^d	601 ± 43^e

[a] Each lipoprotein cholesterol value represents the mean ± S.D. of values from $n = 6$ mice/genotype. Lipoproteins were purified by a combination of ultracentrifugation and FPLC and their lipid content determined as described under "Experimental Procedures." Statistical differences at $p < 0.05$ for each row are indicated by different letters.

root sections are displayed from left to right from LDLr$^{-/-}$, LDLr$^{-/-}$, PCPE2$^{-/-}$, and LDLr$^{-/-}$, apoA-I$^{-/-}$ mice, respectively. The neutral lipid staining is expressed as the percent Oil Red O lesion area in Fig. 2*B* and as total Oil Red O lesion area as μm^2 in Fig. 2*C*. These data indicate that the LDLr$^{-/-}$, PCPE2$^{-/-}$ mouse aorta showed a statistically significant ~46% increase in aortic lipid accumulation compared with LDLr$^{-/-}$ mice, regardless of how the lesion area was expressed. Interestingly, LDLr$^{-/-}$, PCPE2$^{-/-}$ mouse aortic roots accumulated as much neutral lipid as did diet-fed LDLr$^{-/-}$, apoA-I $^{-/-}$ mice (46, 47, 67), which do not express any apoA-I and lack tradi-

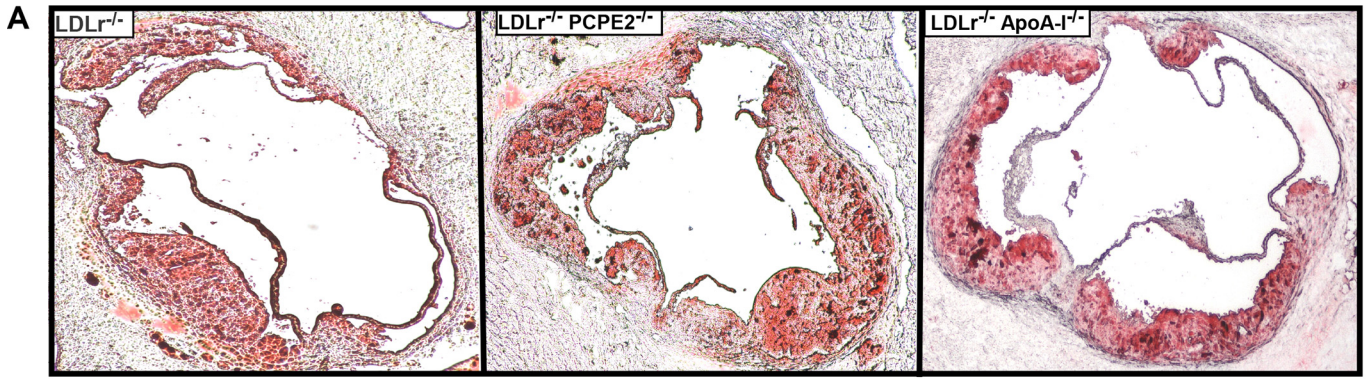

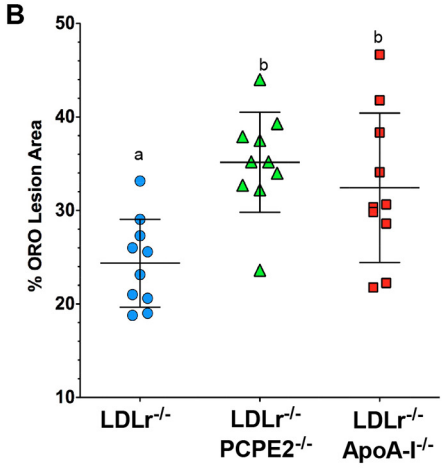

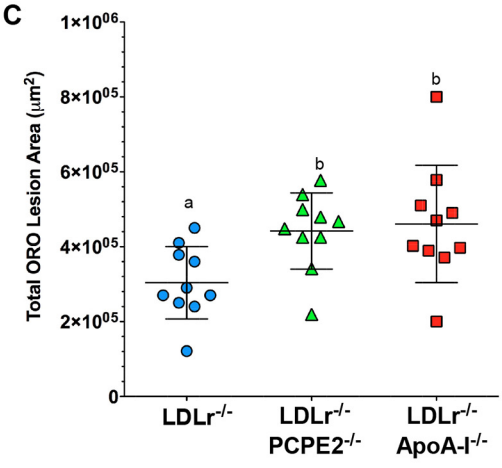

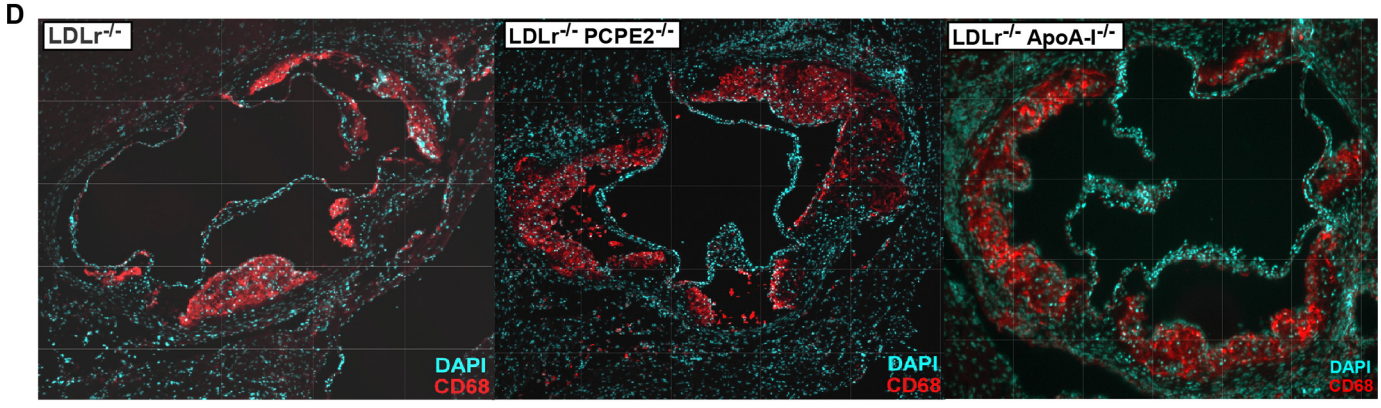

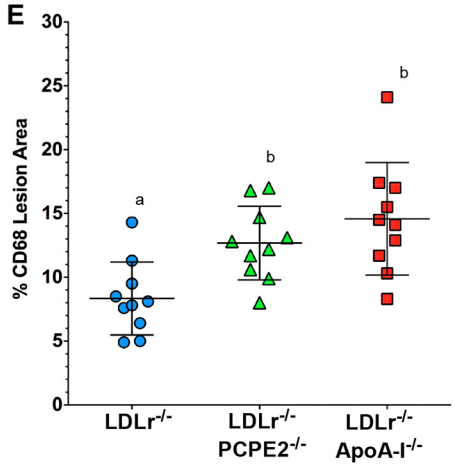

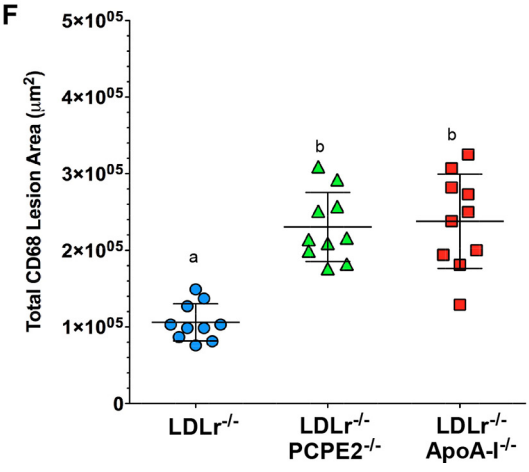

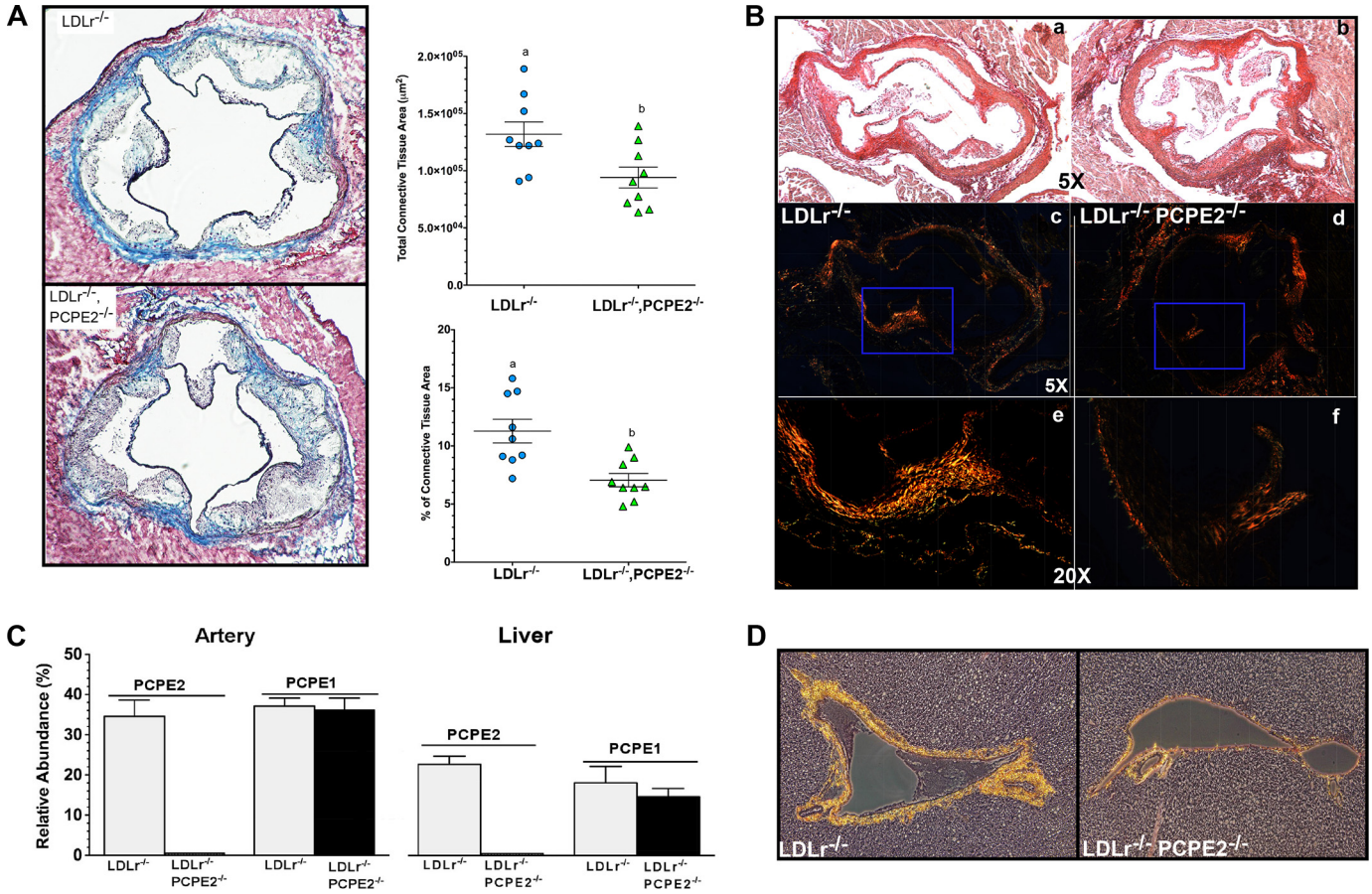

FIGURE 3. **PCPE2 deficiency decreases collagen content in aorta and liver.** *A*, representative aortic root sections following Masson's trichrome staining. Sections were obtained from LDLr$^{-/-}$ and LDLr$^{-/-}$, PCPE2$^{-/-}$ mice fed an atherogenic diet for 12 weeks. Quantification of the absolute connective tissue area and the percent of total collagen content per aortic area is shown adjacent to representative sections from each genotype. Data represent the mean ± S.D. of $n = 10$ male mice/group. Different letters indicate statistical significance at $p < 0.05$. *B*, representative aortic root sections following picrosirius red staining for LDLr$^{-/-}$ in *a*, *c*, and *e* and for LDLr$^{-/-}$, PCPE2$^{-/-}$ in *b*, *d*, and *f*. Bright field ×5 images are shown in *a* and *b*. *c–f*, polarized images at ×5 are shown in *c* and *d* and in the *blue boxed regions* at ×20 in *e* and *f*. *C*, relative mRNA abundance for PCPE2 and PCPE1 in artery (*left*) compared with the liver (*right*) for LDLr$^{-/-}$ mice (*gray bar*) and LDLr$^{-/-}$, PCPE2$^{-/-}$ (*black bar*) mice fed an atherogenic diet. *D*, representative sections of liver from an atherogenic diet-fed LDLr$^{-/-}$ and LDLr$^{-/-}$, PCPE2 mouse stained with picrosirius red and viewed using polarized light to show the birefringence of the collagen fibers.

tionally defined HDL particles in their plasma. Taken together, these results show that higher concentrations of enlarged HDL in LDLr$^{-/-}$, PCPE2$^{-/-}$ mice do not offer significant protection against the progression of atherosclerosis. Furthermore, aortic lipid deposition in LDLr$^{-/-}$, PCPE2$^{-/-}$ mice could not be distinguished from that seen in mice having no apoA-I-associated HDL, suggesting that the HDL particles in LDLr$^{-/-}$, PCPE2$^{-/-}$ mice are dysfunctional in nature.

Staining for the presence of CD68+ cells in the aortic root is commonly used as a marker for macrophage infiltration. Representative stained aortic root sections are shown in Fig. 2*D*: LDLr$^{-/-}$, LDLr$^{-/-}$, PCPE2$^{-/-}$, and LDLr$^{-/-}$, apoA-I$^{-/-}$ mice displayed from left to right, respectively. CD68+ staining is expressed as the percent of CD68+ area in Fig. 2*E* and as total CD68+ area in μm^2 in Fig. 2*F*. As observed with neutral lipid staining, LDLr$^{-/-}$, PCPE2$^{-/-}$ and LDLr$^{-/-}$, apoA-I$^{-/-}$ mouse aortas had about a ~45% increase in CD68+ staining cells compared with aortas from LDLr$^{-/-}$ mice.

Reduced Collagen Content in PCPE2-deficient Mice—Given the reported enhancer properties of PCPE2 on BMP1 catalytic function (68, 69), we measured the connective tissue content in the aortic root using Masson's trichrome. Fig. 3*A* shows representative aortic roots sections from 12-week diet-fed LDLr$^{-/-}$ and LDLr$^{-/-}$, PCPE2$^{-/-}$ mice. Adjacent to each section is the quantification of the connective tissue content, as shown by *dark blue* staining (Fig. 3*A*) for each genotype. Whether the data were calculated as the percent of connective tissue area or as total connective tissue area (μm^2), the LDLr$^{-/-}$, PCPE2$^{-/-}$ aorta had ~28% less connective tissue than the LDLr$^{-/-}$ aorta using Masson's trichrome staining. Because collagen types I

FIGURE 2. **PCPE2 deficiency exacerbates atherosclerosis despite elevated HDL cholesterol levels.** *A*, representative aortic root sections stained with Oil Red O from 12 weeks atherogenic diet-fed LDLr$^{-/-}$, LDLr$^{-/-}$ PCPE2$^{-/-}$, and LDLr$^{-/-}$, apoA-I$^{-/-}$ mice. *B* and *C*, quantification of the atherosclerotic lesion area as a percentage of the total aortic area (*B*) and the total lesion area in μm^2 (*C*). *D*, representative aortic root sections stained with fluorescently labeled antibodies to CD68, a macrophage marker, from 12 weeks atherogenic diet-fed LDLr$^{-/-}$ mice, LDLr$^{-/-}$,PCPE2$^{-/-}$ mice, and LDLr$^{-/-}$, apoA-I$^{-/-}$ mice. *E* and *F*, quantification of the macrophage content was performed by measuring CD68+ staining over background as a percentage of the total lesion area (*E*) and of the total lesion area in μm^2 (*F*). Data represent the mean ± S.D. of $n = 10$ male mice/group. *Different letters* indicate statistical significance at $p < 0.05$. The fluorescence background threshold was set to the intensity of sections receiving the fluorescently tagged secondary antibody but no CD68 primary antibody.

and III are prevalent in mouse heart and aorta, it follows that the regulation of procollagen processing must play an important role in normal tissue maintenance during disease progression (70). The reduction in LDLr$^{-/-}$, PCPE2$^{-/-}$ aortic root connective tissue was confirmed by the picrosirius red staining of paraffin-embedded aortic root sections show in Fig. 3*B*, *a–f*. In Fig. 3*B*, *a*, *c*, and *e*, different views are offered of a representative slide taken from LDLr$^{-/-}$ mouse aortic root, whereas the views in *b*, *d*, and *f* are from LDLr$^{-/-}$, PCPE2$^{-/-}$ mouse aortic root. Fig. 3*B*, *a* and *b*, shows stained aortic root at ×5 magnification using light microscopy, and *c* and *d panels* show the same slide but under polarizing filters. Fig. 3*B*, *e* and *f*, shows the same slides as above but at a ×20 magnification under polarizing filters, as indicated by the *boxed areas* in *c* and *d*. The birefringence of collagen fibers under polarized light shows a shift in color between the various components, red, orange, yellow, and green, and represents the order of decreasing thickness of the fibers. In this case, the LDLr$^{-/-}$, PCPE2$^{-/-}$ mouse aortic root appears to have significantly less birefringence of all thicknesses of collagen fibers when compared with the LDLr$^{-/-}$ aortic root, again confirming the results of the Masson's trichrome staining. Because PCPE1 is highly similar in structure and function to PCPE2 with respect to procollagen processing, we examined whether the expression of PCPE1 might be elevated in the PCPE2-deficient state. Fig. 3*C* compares PCPE1 and PCPE2 mRNA expression in the artery and liver from the two genotypes of mice. No elevation of PCPE1 was seen in either tissue in light of the absence of PCPE2, although these results do show significant expression of both PCPE1 and PCPE2 in the liver of LDLr$^{-/-}$ mice.

Based on the mRNA expression data we then examined the picrosirius staining of collagen fibers in the hepatic triad of livers from LDLr$^{-/-}$, PCPE2$^{-/-}$ and LDLr $^{-/-}$ mice (shown in Fig. 3*D*). Here, under polarizing light the picrosirius-stained hepatic portal triad from LDLr$^{-/-}$, PCPE2$^{-/-}$ mice was compared with that from LDLr$^{-/-}$ mice and showed that both the thickness and amount of collagen are significantly reduced in LDLr$^{-/-}$, PCPE2$^{-/-}$ mice.

PCPE2 Was Not Essential for in Vivo Pro-apoA-I Processing—PCPE2 had been reported to enhance the BMP1-mediated cleavage of propeptides from procollagen (27, 29, 71) during assembly in the extracellular matrix. These studies suggest that cleavage of apoA-I's propeptide is the rate-limiting step to form nHDL (39, 71, 72) and the primary defect in PCPE2-deficient mice. Investigators have hypothesized that if PCPE2 and BMP1 work together to remove the pro-segment of pro-apoA-I, then HDL concentrations in mice lacking PCPE2 expression might be affected. Francone *et al.* (44), having measured HDL apoA-I from PCPE2-deficient mice by isoelectric focusing and mass spectrometry, report an elevation in the amount of plasma pro-apoA-I over mature apoA-I.

To investigate this effect further, we first measured the ratio of intact pro-apoA-I to mature apoA-I in plasma HDL from PCPE2-deficient mice by mass spectrometric analyses. Fig. 4, *A* and *B*, shows the masses of directly infused delipidated apoA-I from the plasma of C57BL/6 (*A*) and PCPE2$^{-/-}$ mice (*B*), respectively, after transformation of the electrospray spectrum. These results demonstrate that in both samples the most abundant mass was consistent with mature mouse apoA-I (27,950 ± 1.4 Da (73)), with only a small amount of mouse pro-apoA-I (28,815 ± 1.4 Da), which includes the mass of the pro-sequence WHVWQQ.

To quantify the amount of pro-apoA-I in plasma, the unique T1 peptide for the mature apoA-I (DEPQSQWDK) tryptic peptide and T1 for pro-apoA-I (WHVWQQDEPQSQWDK), which includes the additional six pro-amino acids, were synthesized and used as standards. The sequence of each synthetic peptide was verified by MS/MS sequencing, and then LC/MS was used to establish the retention times and ionizability of the two different T1 peptides. The ion-current ratio of equal molar amounts of the two synthetic T1 peptides, $T1_{apoA\text{-}I}/T1_{pro\text{-}apoA\text{-}I}$, was found to be 1.07.

Aliquots of mouse plasma were separated on 12% SDS-PAGE. The gel band corresponding to apoA-I at ~28,000 Da was excised and subjected to in-gel digestion using trypsin (51). Following digestion, peptides were exhaustively extracted from the gel slice, separated by reverse-phase HPLC, and identified by monitoring the +2 charge state of each peptide (566.75 *m/z* for mature apoA-I and 998.95 *m/z* for pro-apoA-I). Fig. 4 shows the summed selective ion electrospray mass chromatograms for apoA-I from C57BL/6 (*C*) and PCPE2$^{-/-}$ mouse plasma (*D*). Note that the distribution of both pro- and mature apoA-I was virtually identical for both genotypes. The critical factor for this analysis is that the molar ion intensities of each peptide were nearly identical; therefore, the measured ion intensities could be used to quantify the relative amount of each peptide. This interpretation of our data completely changes the interpretation based on a previous study (44) that reported an elevation in the amount of pro-apoA-I. Thus, our studies suggest that the role of PCPE2 in HDL enlargement is not due to the conversion of pro-apoA-I to mature apoA-I. Overall, we found that both genotypes had very little (~4%) pro-apoA-I, and these results suggest that although PCPE2 may enhance pro-apoA-I processing *in vitro*, *in vivo* the absence of PCPE2 does not appear to be rate-limiting.

PCPE2 Affects HDL ApoA-I Catabolism Rates—To investigate the possibility that increased concentrations of enlarged HDL in plasma were related to the reduced catabolism of plasma HDL in PCPE2-deficient mice, HDL was purified from the plasma of diet-fed LDLr$^{-/-}$ and LDLr$^{-/-}$, PCPE2$^{-/-}$ mice using a combination of ultracentrifugation and FPLC and then radiolabeled with ^{125}I. Purified ^{125}I-labeld HDL particles were injected into diet-fed recipient mice, and the disappearance of radioactivity from plasma was followed over time, as shown in Fig. 5, *A* and *B*. ^{125}I-labeled HDL from LDLr$^{-/-}$ mice injected into LDLr$^{-/-}$ mice had a fractional catabolic rate (FCR) of 0.106 ± 0.010 pools/h as compared with a FCR of 0.076 ± 0.011 when the same HDL was injected into LDLr$^{-/-}$, PCPE2$^{-/-}$ mice (mean ± S.D. of $n = 3$ mice). A similar trend was observed when ^{125}I-labeled HDL from LDLr$^{-/-}$, PCPE2$^{-/-}$ mice was injected into LDLr$^{-/-}$ *versus* LDLr$^{-/-}$, PCPE2$^{-/-}$ mice, resulting in an FCR of 0.097 ± 0.030 *versus* 0.062 ± 0.008, respectively. From these data it appears the rate of turnover for HDL isolated from LDLr$^{-/-}$ or LDLr$^{-/-}$, PCPE2$^{-/-}$ mice was a function of the recipient genotype and not a result of HDL particle origin. In conclusion, these results suggest that PCPE2

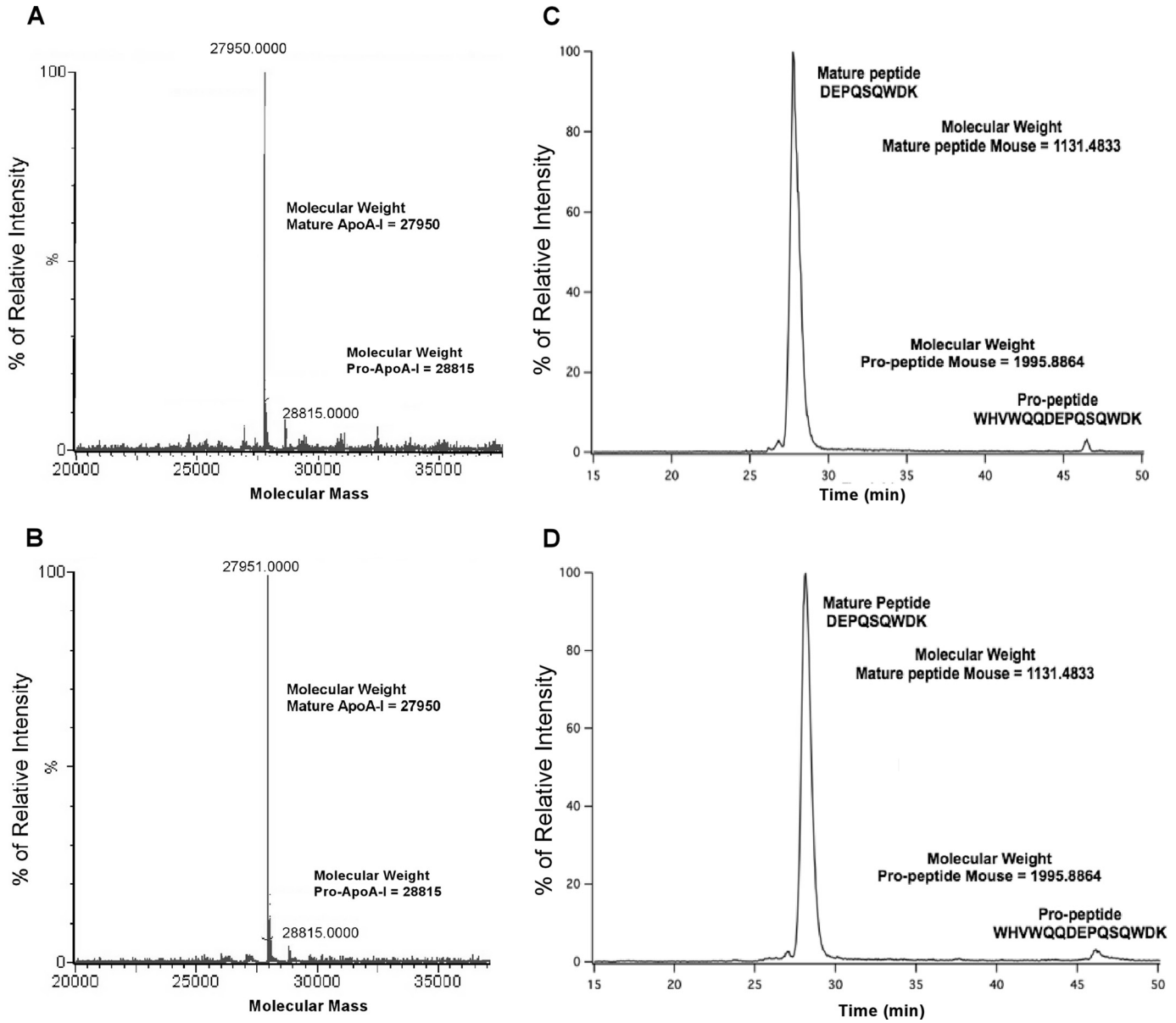

FIGURE 4. **Mass spectrometric analysis and the ratio of mature to pro-apoA-I in HDL from PCPE2$^{-/-}$ mouse plasma.** *A* and *B*, molecular masses of HDL apoA-I after maximum entropy transformation of the electrospray spectrum of FPLC purified HDL apoA-I from chow-fed C57BL/6 mice (*A*) and PCPE2$^{-/-}$ mice (*B*). The most abundant mass in each spectrum was identical within the ±1.4 Da S.D. to the mass of mature mouse apoA-I at 27,950 Da. The minor spectrum peak is consistent with the mass of mouse pro-apoA-I at 28,815 Da. *C* and *D*, the relative intensity of apoA-I tryptic peptides from LC-MS/MS analysis. ApoA-I from whole mouse plasma was separated by 12% SDS-PAGE followed by in-gel trypsin digest and then analyzed for the N-terminal tryptic pro-apoA-I peptide and mature apoA-I peptide: C57BL/6 mouse plasma (*C*) and PCPE2$^{-/-}$ mouse plasma (*D*) as described under "Experimental Procedures." Peptides were separated by reverse-phase HPLC and analyzed for tryptic peptide of the N-terminal T1 for mature peptide (*m/z* 1132.48) and the T1 propeptide (*m/z* 1995.88), shown in selective ion chromatograms. The mature murine T1 tryptic peptide has the amino acid sequence DEPQSQWDK, and the unprocessed pro-form has the sequence WHVWQQDEPQSQWDK.

exerts its effects on HDL metabolism by assisting in particle remodeling and/or removal. There was a trend suggesting that the larger LDLr$^{-/-}$, PCPE2$^{-/-}$-derived HDL particles were removed more slowly in both genotypes, but this trend did not reach statistical significance.

PCPE2 and Reverse Cholesterol Transport—As PCPE2 is expressed in the extracellular matrix of mouse liver (29), we next determined how its absence might alter macrophage to liver reverse cholesterol transport (61). To this end, atherogenic diet-fed LDLr$^{-/-}$ and LDLr$^{-/-}$, PCPE2$^{-/-}$ mice received an intraperitoneal injection of [^{3}H]cholesterol-loaded J774 foam cells (61). The amount of [^{3}H]cholesterol appearing in the plasma and feces was measured for 0–48 h, and the results are presented as the percent of injected dose (shown in Fig. 5, *C* and *D*, respectively). Six hours after the [^{3}H]cholesterol-loaded J774 cells were injected, there was a significant difference in the appearance of [^{3}H]cholesterol in plasma between the two genotypes (Fig. 5*C*). LDLr$^{-/-}$, PCPE2$^{-/-}$ mouse plasma showed a 2-fold higher concentration of [^{3}H]cholesterol, which remained relatively constant over the course of the study. In contrast, LDLr$^{-/-}$ mice showed a comparatively slower increase in plasma radioactivity, which reached a maximum by 24 h and then decreased by 48 h. The excretion of neutral [^{3}H]cholesterol in LDLr$^{-/-}$ mouse feces was statistically

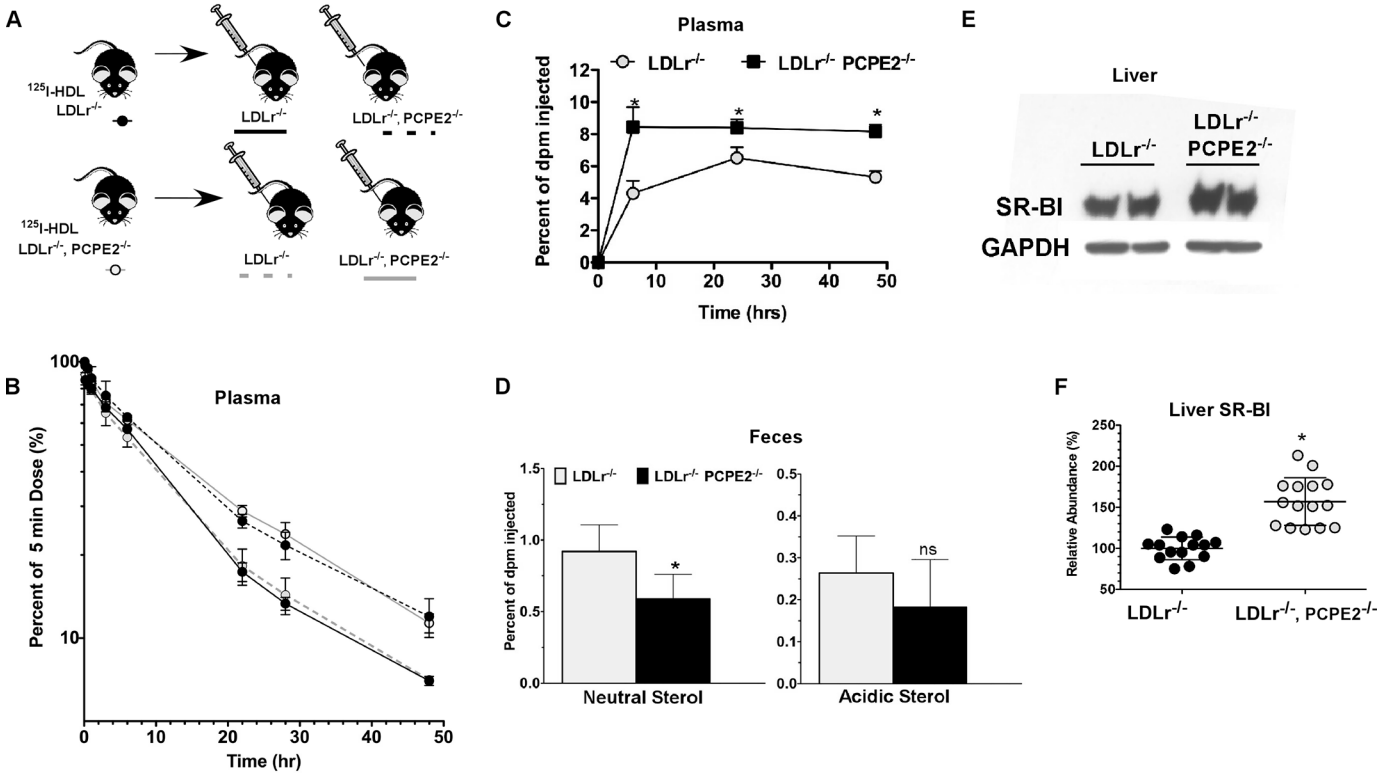

FIGURE 5. **Absence of liver PCPE2 affects HDL-mediated reverse cholesterol transport and SR-BI expression.** *A*, HDL from diet-fed LDLr$^{-/-}$ and LDLr$^{-/-}$, PCPE2$^{-/-}$ mice was purified and then radiolabeled with ^{125}I as described under "Experimental Procedures." Approximately 10×10^6 cpm of ^{125}I-labeled HDL was retro-orbitally injected into atherogenic diet-fed recipient mice of the indicated genotype. Blood was collected from the contralateral retro-orbital sinus at the indicated times. *B*, the FCR of ^{125}I-labeled HDL were determined from plasma decay curves assuming a one-pool model as described under "Experimental Procedures." Data represent the mean ± S.D. of $n = 3$ mice/group. *C*, [^{3}H]cholesterol levels in plasma during macrophage reverse cholesterol transport study in LDLr$^{-/-}$ (*gray circles*) and LDLr$^{-/-}$, PCPE2$^{-/-}$ (*black squares*) mice fed an atherogenic diet. Mice were injected intraperitoneally with [^{3}H]cholesterol-labeled J774 foam cells as described under "Experimental Procedures." *D*, [^{3}H]cholesterol in feces after 0–48 h collection. The numerical data shown is the mean ± S.D. of $n = 5$–6 male mice for each genotype. The *asterisk* indicates statistical significance at $p < 0.001$. *ns*, indicates that the difference was not significant. *E*, an immunoblot analysis of liver SR-BI levels in atherogenic diet-fed mice. *F*, relative mRNA abundance of liver SR-BI in atherogenic diet-fed mice. Data represent the results from $n = 6$–10 male mice/genotype. The liver mRNA abundance of SR-BI in LDLr$^{-/-}$ mouse liver was set at 100%.

greater than that in LDLr$^{-/-}$, PCPE2$^{-/-}$ mouse feces (Fig. 5*D*). Although a trend for greater ^{3}H acidic sterol excretion was seen for LDLr$^{-/-}$ compared with LDLr$^{-/-}$, PCPE2$^{-/-}$ mice, it was not statistically significant. Together, the plasma and fecal analyses indicate that in the absence of PCPE2 less macrophage cholesterol was removed by the RCT pathway to the liver.

Although RCT consists of multiple steps, it is largely dependent on the expression of hepatic SR-BI (74). It is also known that attenuation of SR-B1 in mice results in a substantial increase in HDL plasma levels (10). Based on these facts, we next examined the expression of SR-BI in the liver of LDLr$^{-/-}$, PCPE2$^{-/-}$ mice by both RT-PCR and Western blot analysis (shown in Fig. 5, *E* and *F*). Here an immunoblot probing for mouse SR-B1 using liver extracts from two different mice per genotype shows that SR-B1 levels in LDLr$^{-/-}$, PCPE2$^{-/-}$ mice are approximately twice that in LDLr$^{-/-}$ mouse livers, whereas GAPDH levels are constant. These findings were further supported by RT-PCR analysis showing a greater abundance of SR-BI mRNA in liver from LDLr$^{-/-}$, PCPE2$^{-/-}$ mice compared with controls (Fig. 5*F*), suggesting that both SR-B1 mRNA, as well as protein, is up-regulated in the LDLr$^{-/-}$, PCPE2$^{-/-}$ mouse liver. This outcome was unexpected because our earlier results showed a reduction in RCT and HDL catabolism, consistent with a reduction in SR-BI. These results led us to focus next on measuring the effect of PCPE2 expression on SR-BI function.

PCPE2 Enhances SR-BI Cholesteryl Ester Uptake Function—To determine how PCPE2 expression might affect SR-BI function, we first considered testing primary hepatocytes from LDLr$^{-/-}$, PCPE2$^{-/-}$ and control mice. However, the presence of PCPE2 in the extracellular matrix was not compatible with the use of collagenase during hepatocyte isolation. In addition, reports cautioning against the use of primary hepatocytes when studying SR-BI regulation (75) led us to perform a gain of function study in CHO cells (76). To test the effect of PCPE2 on SR-BI-mediated HDL-cholesteryl ester uptake, we first determined the surface expression of PCPE2 in CHO cells that were either mock-transfected or transfected with a plasmid expressing PCPE2 for 24 h. Fig. 6*A* shows a histogram of PCPE2 surface expression 24 h after transfection measured by flow cytometry. The *dotted line* depicts the expression of PCPE2 in control cells, and the *shaded solid line* depicts the shift in PCPE2 surface expression in PCPE2 transiently transfected CHO cells (Fig. 6*A*). The 2-fold increase (47926 ± 1025 *versus* 21336 ± 525, mean ± S.D., $n = 3$ independent experiments) indicates that PCPE2 transfection significantly increased its expression on the cell surface, consistent with the known function of PCPE2 in the extracellular matrix.

Next, to test the effect of PCPE2 on SR-BI function, CHO cells were mock-transfected or transfected with a construct encoding PCPE2 and then assayed for their ability to take up

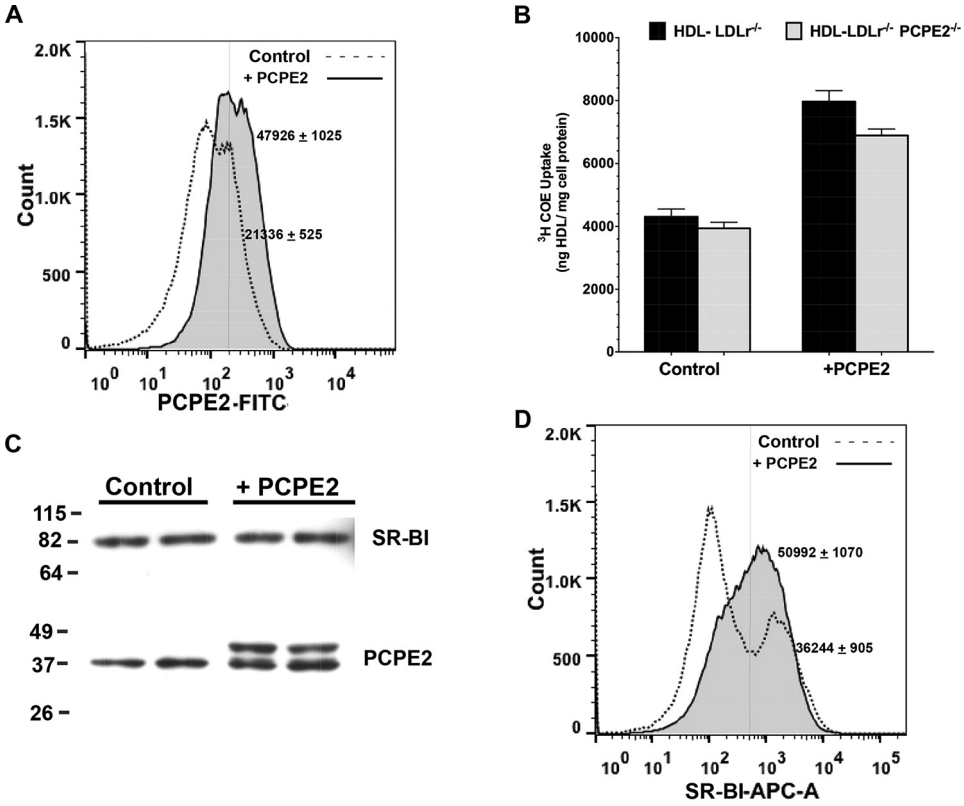

FIGURE 6. **SR-BI functionality is enhanced in the presence of PCPE2.** *A*, a histogram of PCPE2 cell surface expression by flow cytometry. CHO cells were either mock-transfected or control CHO cells (*dotted line*) or transiently transfected with PCPE2 (*shaded solid line*). The next day the cells were stained for surface PCPE2 expression as described under "Experimental Procedures." A 2-fold increase (47926 ± 1025 *versus* 21336 ± 525, mean ± S.D., $n = 3$ independent experiments) in PCPE2 surface expression in transiently transfected cells is consistent with the PCPE2 known location in the extracellular matrix. *B*, the uptake of ^{3}H-COE-labeled HDL by control and PCPE2-overexpressing CHO cells expressed as ng of HDL taken up/mg of cell protein. Confluent wells of CHO cells were either mock-transfected or transfected with a plasmid encoding PCPE2 as described under "Experimental Procedures." The next day the cells were washed and then incubated for 1.5 h with 10 μg of ^{3}H-COE-labeled HDL obtained from either diet-fed LDLr$^{-/-}$ or LDLr$^{-/-}$, PCPE2$^{-/-}$ mouse plasma as described under "Experimental Procedures." The cells were washed extensively, and then the cell pellet was digested in 0.1 N NaOH and its protein and radioactivity content quantified as described under "Experimental Procedures." Each value represents the mean ± S.D. of $n = 3$ wells/condition from three independent experiments. *C*, an immunoblot of SR-BI and PCPE2 protein expression from control and PCPE2-overexpressing CHO cells. Each *lane* contains 25 μg of total protein. *D*, a histogram of SR-BI surface expression in mock (*dotted line*)- and PCPE2-transfected CHO (*shaded solid line*) cells by flow cytometry. Overexpression of PCPE2 leads to a shift to a single population, with a significantly higher frequency of SR-BI per cell (50992 ± 1070 *versus* 36244 ± 905, mean ± S.D., $n = 3$ independent experiments).

HDL-cholesteryl ester. The day after mock or transient transfection with PCPE2, confluent cell monolayers were washed and then incubated with 10 μg of labeled ^{3}H-COE HDL for 1.5 h in triplicate. Following incubation, the monolayer was washed extensively and the cell pellet subjected to radioactivity and protein quantification. Fig. 6*B* shows the results of these studies and suggests that the overexpression of PCPE2 enhanced the uptake of ^{3}H-COE HDL. This increase in SR-BI function appeared to be independent of HDL origin, because HDL particles derived from either LDLr$^{-/-}$ or LDLr$^{-/-}$, PCPE2$^{-/-}$ mice showed a similar extent of ^{3}H-COE uptake.

We next examined the protein extracts from cells that were either mock-transfected or transfected with PCPE2 using immunoblot analysis, as shown in Fig. 6*C*. In this study, the total cellular SR-BI protein was unchanged by PCPE2 overexpression. PCPE2 protein levels were increased with overexpression, as identified by the 1.2-kDa increase in the endogenous molecular mass due to the MycDDK tag on the exogenously expressed PCPE2.

To further explore the mechanism behind PCPE2 enhancement of SR-BI function, mock- and PCPE2-transfected CHO cells were stained and analyzed for SR-BI surface expression using flow cytometry. Fig. 6*D* shows a histogram of surface SR-BI expression in control cells, indicated by the *dotted line*, and in cells overexpressing PCPE2, denoted by a *solid line*. Interestingly, the control cells contain two populations of cells, one characterized by a low surface frequency of SR-BI/cell and a second population with a significantly higher frequency of SR-BI/cell. Upon overexpression of PCPE2, a shift to one population with a significantly higher frequency of SR-BI/cell is observed (50992 ± 1070 *versus* 36244 ± 905, mean ± S.D., $n =$ 3 independent experiments). These results suggest that PCPE2 may act to enhance SR-BI function by promoting or maintaining SR-BI expression on the cell surface.

Discussion

The current studies show for the first time that PCPE2, an extracellular matrix-associated protein, confers an atheroprotective function to HDL *in vivo*. The implication is that in the absence of PCPE2, HDL particles are dysfunctional and cannot protect against the progression of atherosclerosis. In addition, these studies show that the apparent HDL dysfunction results

from reduced HDL-CE catabolism via SR-BI and is not actually due to changes within the particle or its components itself (Fig. 5, *A–D*). Surprisingly, the extent of atherosclerosis in LDLr$^{-/-}$, PCPE2$^{-/-}$ mice was indistinguishable from that in LDLr$^{-/-}$, apoA-I$^{-/-}$ mice, which lack all apoA-I-containing HDL particles (47). Although both LDLr$^{-/-}$, PCPE2$^{-/-}$ and LDLr$^{-/-}$, apoA-I$^{-/-}$ mice had similar extents of atherosclerosis, there was an uncoupling of its progression as it relates to total plasma cholesterol levels (77). LDLr$^{-/-}$, apoA-I$^{-/-}$ mice had no HDL and half the circulating LDL cholesterol levels as diet-fed LDLr$^{-/-}$ mice (46). In contrast, LDLr$^{-/-}$, PCPE2$^{-/-}$ mice had higher HDL cholesterol concentrations and similar LDL cholesterol concentrations relative to LDLr$^{-/-}$ mice but increased atherosclerosis. These findings suggest that the term "dysfunctional HDL," *e.g.* HDL that is not atheroprotective, does not technically apply in this situation. Rather, HDL-related dysfunctionality was caused by obstruction of the RCT at one or more of its individual steps.

There are several mechanistic scenarios for the role of PCPE2. The first is that PCPE2 confers atheroprotection to apoA-I by enhancing BMP1-mediated catalytic cleavage, converting pro-apoA-I to mature apoA-I, and stimulating ABCA1-mediated cholesterol flux (26, 44). However, our studies show conclusively that pro-apoA-I processing was not altered in the case of PCPE2 deficiency (Fig. 4). The absence of PCPE2 did not affect the circulating levels of pro-apoA-I *in vivo*, which remained around 3–6% of total apoA-I for both PCPE2-replete and PCPE2 knock-out mice. Although PCPE2 enhanced pro-apoA-I processing *in vitro* and was shown to have a high affinity for apoA-I using both surface plasmon resonance and selective co-immuno-precipitation (26), its absence *in vivo* did affect the ratio of pro- to mature apoA-I. This was not unexpected, because PCPE2 is not essential for catalytic cleavage of pro-apoA-I by BMP1 (39, 42). Theoretically, PCPE2 may limit BMP1-mediated processing of pro-apoA-I under high substrate conditions, as reported for the processing of procollagen in the heart following chronic pressure overload (70).

Insight into the molecular mechanism of the protective function of PCPE2 comes from our HDL clearance studies (Fig. 5, *A* and *B*), where the fractional clearance of HDL was delayed in PCPE2-deficient mice, regardless of the source of the HDL. A slower catabolic turnover resulted in increased HDL concentration, which ultimately caused HDL particle enlargement (Fig. 1). In mice, increased HDL size and concentration is a hallmark of SR-B1 deficiency (78). Hepatic specific SR-B1-deficient mice were reported to have higher plasma HDL levels than the controls, with greater aortic lesion formation. Because hepatic SR-B1 mediates selective uptake of HDL-cholesteryl esters and their removal from circulation for excretion into bile (74), it was concluded that in mice SR-BI is a positive regulator of macrophage RCT. As seen in genetically modified mice, humans with genetic variants in SR-BI show a reduced capacity to efflux CE, which leads to greater HDL plasma concentrations (79–82) and a greater risk for CVD. Our study showed a macrophage to fecal RCT rate significantly lower in LDLr$^{-/-}$, PCPE2$^{-/-}$ mice and similar to that reported for SR-BI knock-out mice. Interestingly, this lower rate occurred despite a 2-fold higher level of SR-BI protein in the livers of LDLr$^{-/-}$, PCPE2$^{-/-}$ mice (Fig. 5, *C–F*).

The impact of PCPE2 on liver SR-BI functionality was demonstrated by slower plasma HDL-CE turnover, reduced macrophage cholesterol to fecal deliver, and increased plasma HDL size and concentration. Despite elevations in plasma HDL, the aortic lipid and immune cell infiltration was greater in the absence of PCPE2, highlighting the importance of aortic SR-BI in preventing the progression of atherosclerosis. These results prompted us to consider how PCPE2 might influence hepatic SR-BI function.

Transient transfection of CHO cells with PCPE2 gave a 2-fold increase in PCPE2 surface expression (Fig. 6, *A* and *C*) and an almost 2-fold increase in the uptake of ^{3}H-COE from labeled HDL (Fig. 6*B*). Overexpression of PCPE2 in CHO cells did not change total SR-BI protein levels but did increase the amount of SR-B1 protein measured on the surface of transfected cells (Fig. 6*D*). In contrast, liver SR-BI expression in PCPE2 knock-out mice was increased 2-fold. The absence of an increase in SR-B1 protein following transfection may be ascribed to the transient nature of the *in vitro* experiment.

Our studies also provide evidence for a profound reduction in connective tissue content in both the aortic root and the hepatic triad in mice lacking PCPE2 (Fig. 3, *A–D*). PCPE2 enhances procollagen processing and is abundantly expressed in the heart, aorta, adipose tissue, and trabecular meshwork (27, 29, 38). The expression of PCPE1, which is related to PCPE2, was not increased as a result of PCPE2 deletion (Fig. 3, *C* and *D*) and did not substitute for PCPE2 in arterial tissue. The consequences of these changes in connective tissue content are not known at this time but may be related to the positioning and or stabilization of SR-B1 on the cell surface.

The mechanistic steps involved in SR-BI-mediated aortic cholesterol homeostasis have been studied for years, but questions still remain. How SR-B1 mediates selective CE removal from HDL at the cell surface, leaving lipid-poor apoA-I after transferring CE into the cell, remains unresolved. Nevertheless our results strongly suggest that SR-BI-mediated ^{3}H-COE removal from HDL is facilitated by surface-bound PCPE2. The mechanism of the influence of PCPE2 on SR-BI uptake of HDL-CE may involve promoting the oligomerization of SR-BI with itself, with PCPE2, or with other proteins. Previous studies have demonstrated that SR-BI forms dimers and tetramers on the cell surface necessary for its function (83–85). Oligomerization has been postulated to form a hydrophobic channel that facilitates the selective delivery of CE from HDL to the cell. Although putative SR-BI oligomerization domains are thought to localize to the transmembrane segment, it has been suggested that the extracellular domains of SR-BI may also contribute to oligomerization (86). The shift in SR-BI surface stain intensity (Fig. 6*D*) suggests a significant change in antibody binding properties and, therefore, a change in the conformation of amino acid region 338–440.

Alternative explanations for the action of PCPE2 on SR-BI include the postulation that PCPE2 binds and sequesters SR-B1 at the cell surface. Previous studies have reported that the intracellular adaptor protein PDZK1 binds the C terminus of SR-BI and is required for receptor function (87, 88). In an analogous

way, PCPE2 may provide scaffolding or tethering at the cell surface, promoting association of SR-B1 with HDL-CE. Another possibility would be that PCPE2 is involved in SR-BI endocytosis (89–92). Yet another plausible mechanism is based on the previously shown ability of PCPE2 to bind apoA-I (26); here PCPE2 would interact with apoA-I bound to HDL, thereby altering the protein conformation and in turn enhancing CE removal. As the current report provides a solid foundation for our understanding of PCPE2 function, additional studies will be needed to examine the structures of and potential interactions between PCPE2 and SR-BI, allowing insights into the mechanisms through which PCPE2 controls SR-BI-mediated HDL-CE uptake.

In conclusion, our studies show for the first time that an extracellular matrix protein, PCPE2, is essential for the integrity of the HDL-mediated CE transport system. These studies also show that simply measuring plasma HDL concentration or its associated components in order to assess one's risk of CVD can be misleading. Rather, a combination of HDL production, catabolism, and concentration is essential for a precise analysis of HDL function. The novel finding is that PCPE2 contributes to SR-BI function by enhancing the rate of HDL-CE uptake, thereby stimulating the RCT pathway. Because the molecular events that drive the selective uptake of CE from HDL particles via SR-BI have yet to be completely delineated, the questions generated by this work will lead to new studies designed to define those mechanisms. Overall, these studies will ultimately lead to a precise understanding of how SR-BI mediates selective CE uptake and provide new insights into how extracellular matrix-associated proteins, such as PCPE2, protect against the development of atherosclerosis.

Acknowledgments—The mass spectrometers used for these studies were acquired with funds from several agencies: TSQ Discovery Max LC-MS/MS and Advion Nanomate from North Carolina Biotechnology Grant 2007-IDG-1021, TSQ Quantum XLS GC-MS/MS from National Institutes of Health (NIH) Shared Instrumentation Grant 1S10RR027940, and Waters Q-TOF mass spectrometer from NIH Shared Instrumentation Grant 1S10RR17846. The MS analyses were performed in the Mass Spectrometer Facility of the Comprehensive Cancer Center of Wake Forest University School of Medicine, supported in part by NIH Grant 5P30CA12197 from NCI.

References

1. Kwiterovich, P. O., Jr. (1998) The antiatherogenic role of high-density lipoprotein cholesterol. *Am. J. Cardiol.* **82,** 13Q–21Q
2. Boden, W. E. (2000) High-density lipoprotein cholesterol as an independent risk factor in cardiovascular disease: assessing the data from Framingham to the Veterans Affairs High-density Lipoprotein Intervention Trial. *Am. J. Cardiol.* **86,** 19L–22L
3. Castelli, W. P., Doyle, J. T., Gordon, T., Hames, C. G., Hjortland, M. C., Hulley, S. B., Kagan, A., and Zukel, W. J. (1977) HDL cholesterol and other lipids in coronary heart disease: the cooperative lipoprotein phenotyping study. *Circulation* **55,** 767–772
4. Patel, S., Drew, B. G., Nakhla, S., Duffy, S. J., Murphy, A. J., Barter, P. J., Rye, K. A., Chin-Dusting, J., Hoang, A., Sviridov, D., Celermajer, D. S., and Kingwell, B. A. (2009) Reconstituted high-density lipoprotein increases plasma high-density lipoprotein anti-inflammatory properties and cholesterol efflux capacity in patients with type 2 diabetes. *J. Am. Coll. Cardiol.* **53,** 962–971
5. Oram, J. F., and Vaughan, A. M. (2000) ABCA1-mediated transport of cellular cholesterol and phospholipids to HDL apolipoproteins. *Curr. Opin. Lipidol.* **11,** 253–260
6. Iatan, I., Bailey, D., Ruel, I., Hafiane, A., Campbell, S., Krimbou, L., and Genest, J. (2011) Membrane microdomains modulate oligomeric ABCA1 function: impact on apoAI-mediated lipid removal and phosphatidylcholine biosynthesis. *J. Lipid Res.* **52,** 2043–2055
7. Denis, M., Haidar, B., Marcil, M., Bouvier, M., Krimbou, L., and Genest, J., Jr. (2004) Molecular and cellular physiology of apolipoprotein A-I lipidation by the ATP-binding cassette transporter A1 (ABCA1). *J. Biol. Chem.* **279,** 7384–7394
8. Wang, S., Gulshan, K., Brubaker, G., Hazen, S. L., and Smith, J. D. (2013) ABCA1 mediates unfolding of apolipoprotein AI N terminus on the cell surface before lipidation and release of nascent high-density lipoprotein. *Arterioscler. Thromb. Vasc. Biol.* **33,** 1197–1205
9. Nagata, K. O., Nakada, C., Kasai, R. S., Kusumi, A., and Ueda, K. (2013) ABCA1 dimer-monomer interconversion during HDL generation revealed by single-molecule imaging. *Proc. Natl. Acad. Sci. U.S.A.* **110,** 5034–5039
10. Trigatti, B., Rayburn, H., Viñals, M., Braun, A., Miettinen, H., Penman, M., Hertz, M., Schrenzel, M., Amigo, L., Rigotti, A., and Krieger, M. (1999) Influence of the high density lipoprotein receptor SR-BI on reproductive and cardiovascular pathophysiology. *Proc. Natl. Acad. Sci. U.S.A.* **96,** 9322–9327
11. Cuchel, M., Lund-Katz, S., de la Llera-Moya, M., Millar, J. S., Chang, D., Fuki, I., Rothblat, G. H., Phillips, M. C., and Rader, D. J. (2010) Pathways by which reconstituted high-density lipoprotein mobilizes free cholesterol from whole body and from macrophages. *Arterioscler. Thromb. Vasc. Biol.* **30,** 526–532
12. Rye, K. A., and Barter, P. J. (2004) Formation and metabolism of preβ-migrating, lipid-poor apolipoprotein A-I. *Arterioscler. Thromb. Vasc. Biol.* **24,** 421–428
13. Khera, A. V., Cuchel, M., de la Llera-Moya, M., Rodrigues, A., Burke, M. F., Jafri, K., French, B. C., Phillips, J. A., Mucksavage, M. L., Wilensky, R. L., Mohler, E. R., Rothblat, G. H., and Rader, D. J. (2011) Cholesterol efflux capacity, high-density lipoprotein function, and atherosclerosis. *N. Engl. J. Med.* **364,** 127–135
14. de la Llera-Moya, M., Drazul-Schrader, D., Asztalos, B. F., Cuchel, M., Rader, D. J., and Rothblat, G. H. (2010) The ability to promote efflux via ABCA1 determines the capacity of serum specimens with similar high-density lipoprotein cholesterol to remove cholesterol from macrophages. *Arterioscler. Thromb. Vasc. Biol.* **30,** 796–801
15. Rohatgi, A., Khera, A., Berry, J. D., Givens, E. G., Ayers, C. R., Wedin, K. E., Neeland, I. J., Yuhanna, I. S., Rader, D. R., de Lemos, J. A., and Shaul, P. W. (2014) HDL cholesterol efflux capacity and incident cardiovascular events. *N. Engl. J. Med.* **371,** 2383–2393
16. Sorci-Thomas, M. G., Owen, J. S., Fulp, B., Bhat, S., Zhu, X., Parks, J. S., Shah, D., Jerome, W. G., Gerelus, M., Zabalawi, M., and Thomas, M. J. (2012) Nascent high density lipoproteins formed by ABCA1 resemble lipid rafts and are structurally organized By three ApoA-I monomers. *J. Lipid Res.* **53,** 1890–1909
17. Sorci-Thomas, M. G., and Thomas, M. J. (2013) Why targeting HDL should work as a therapeutic tool, but has not. *J. Cardiovasc. Pharmacol.* **62,** 239–246
18. Vedhachalam, C., Duong, P. T., Nickel, M., Nguyen, D., Dhanasekaran, P., Saito, H., Rothblat, G. H., Lund-Katz, S., and Phillips, M. C. (2007) Mechanism of ATP-binding cassette transporter A1-mediated cellular lipid efflux to apolipoprotein A-I and formation of high density lipoprotein particles. *J. Biol. Chem.* **282,** 25123–25130
19. Sorci-Thomas, M. G., and Thomas, M. J. (2012) High density lipoprotein biogenesis, cholesterol efflux, and immune cell function. *Arterioscler. Thromb. Vasc. Biol.* **32,** 2561–2565
20. Vedhachalam, C., Ghering, A. B., Davidson, W. S., Lund-Katz, S., Rothblat, G. H., and Phillips, M. C. (2007) ABCA1-induced cell surface binding sites for ApoA-I. *Arterioscler. Thromb. Vasc. Biol.* **27,** 1603–1609
21. Hozoji, M., Kimura, Y., Kioka, N., and Ueda, K. (2009) Formation of two intramolecular disulfide bonds is necessary for ApoA-I-dependent cholesterol efflux mediated by ABCA1. *J. Biol. Chem.* **284,** 11293–11300

22. Wang, N., Chen, W., Linsel-Nitschke, P., Martinez, L. O., Agerholm-Larsen, B., Silver, D. L., and Tall, A. R. (2003) A PEST sequence in ABCA1 regulates degradation by calpain protease and stabilization of ABCA1 by apoA-I. *J. Clin. Invest.* **111,** 99–107
23. Wang, N., Silver, D. L., Costet, P., and Tall, A. R. (2000) Specific binding of ApoA-I, enhanced cholesterol efflux, and altered plasma membrane morphology in cells expressing ABC1. *J. Biol. Chem.* **275,** 33053–33058
24. Curtiss, L. K., Valenta, D. T., Hime, N. J., and Rye, K. A. (2006) What is so special about apolipoprotein AI in reverse cholesterol transport? *Arterioscler. Thromb. Vasc. Biol.* **26,** 12–19
25. Chirackal Manavalan, A. P., Kober, A., Metso, J., Lang, I., Becker, T., Hasslitzer, K., Zandl, M., Fanaee-Danesh, E., Pippal, J. B., Sachdev, V., Kratky, D., Stefulj, J., Jauhiainen, M., and Panzenboeck, U. (2014) Phospholipid transfer protein is expressed in cerebrovascular endothelial cells and involved in high density lipoprotein biogenesis and remodeling at the blood-brain barrier. *J. Biol. Chem.* **289,** 4683–4698
26. Zhu, J., Gardner, J., Pullinger, C. R., Kane, J. P., Thompson, J. F., and Francone, O. L. (2009) Regulation of apoAI processing by procollagen C-proteinase enhancer-2 and bone morphogenetic protein-1. *J. Lipid Res.* **50,** 1330–1339
27. Xu, H., Acott, T. S., and Wirtz, M. K. (2000) Identification and expression of a novel type I procollagen C-proteinase enhancer protein gene from the glaucoma candidate region on 3q21-q24. *Genomics* **66,** 264–273
28. Steiglitz, B. M., and Greenspan, D. S. (2001) Assignment of the mouse Pcolce2 gene, which encodes procollagen C-proteinase enhancer protein 2, to chromosome 9 and localization of PCOLCE2 to human chromosome 3q23. *Cytogenet. Cell Genet.* **95,** 244–245
29. Steiglitz, B. M., Keene, D. R., and Greenspan, D. S. (2002) PCOLCE2 encodes a functional procollagen C-proteinase enhancer (PCPE2) that is a collagen-binding protein differing in distribution of expression and post-translational modification from the previously described PCPE1. *J. Biol. Chem.* **277,** 49820–49830
30. Vadon-Le Goff, S., Kronenberg, D., Bourhis, J. M., Bijakowski, C., Raynal, N., Ruggiero, F., Farndale, R. W., Stöcker, W., Hulmes, D. J., and Moali, C. (2011) Procollagen C-proteinase enhancer stimulates procollagen processing by binding to the C-propeptide region only. *J. Biol. Chem.* **286,** 38932–38938
31. Kronenberg, D., Vadon-Le Goff, S., Bourhis, J. M., Font, B., Eichenberger, D., Hulmes, D. J., and Moali, C. (2009) Strong cooperativity and loose geometry between CUB domains are the basis for procollagen c-proteinase enhancer activity. *J. Biol. Chem.* **284,** 33437–33446
32. Blanc, G., Font, B., Eichenberger, D., Moreau, C., Ricard-Blum, S., Hulmes, D. J., and Moali, C. (2007) Insights into how CUB domains can exert specific functions while sharing a common fold: conserved and specific features of the CUB1 domain contribute to the molecular basis of procollagen C-proteinase enhancer-1 activity. *J. Biol. Chem.* **282,** 16924–16933
33. Gaboriaud, C., Gregory-Pauron, L., Teillet, F., Thielens, N. M., Bally, I., and Arlaud, G. J. (2011) Structure and properties of the Ca(2+)-binding CUB domain, a widespread ligand-recognition unit involved in major biological functions. *Biochem. J.* **439,** 185–193
34. Teillet, F., Gaboriaud, C., Lacroix, M., Martin, L., Arlaud, G. J., and Thielens, N. M. (2008) Crystal structure of the CUB1-EGF-CUB2 domain of human MASP-1/3 and identification of its interaction sites with mannan-binding lectin and ficolins. *J. Biol. Chem.* **283,** 25715–25724
35. Brier, S., Pflieger, D., Le Mignon, M., Bally, I., Gaboriaud, C., Arlaud, G. J., and Daniel, R. (2010) Mapping surface accessibility of the C1r/C1s tetramer by chemical modification and mass spectrometry provides new insights into assembly of the human C1 complex. *J. Biol. Chem.* **285,** 32251–32263
36. Bally, I., Rossi, V., Lunardi, T., Thielens, N. M., Gaboriaud, C., and Arlaud, G. J. (2009) Identification of the C1q-binding Sites of Human C1r and C1s: a refined three-dimensional model of the C1 complex of complement. *J. Biol. Chem.* **284,** 19340–19348
37. Bekhouche, M., Kronenberg, D., Vadon-Le Goff, S., Bijakowski, C., Lim, N. H., Font, B., Kessler, E., Colige, A., Nagase, H., Murphy, G., Hulmes, D. J., and Moali, C. (2010) Role of the netrin-like domain of procollagen C-proteinase enhancer-1 in the control of metalloproteinase activity. *J. Biol. Chem.* **285,** 15950–15959
38. Weiss, T., Ricard-Blum, S., Moschcovich, L., Wineman, E., Mesilaty, S., and Kessler, E. (2010) Binding of procollagen C-proteinase enhancer-1 (PCPE-1) to heparin/heparan sulfate: properties and role in PCPE-1 interaction with cells. *J. Biol. Chem.* **285,** 33867–33874
39. Chau, P., Fielding, P. E., and Fielding, C. J. (2007) Bone morphogenetic protein-1 (BMP-1) cleaves human proapolipoprotein A1 and regulates its activation for lipid binding. *Biochemistry* **46,** 8445–8450
40. Sviridov, D. (2009) Maturation of apolipoprotein A-I: unrecognized health benefit or a forgotten rudiment? *J. Lipid Res.* **50,** 1257–1258
41. Getz, G. S., and Reardon, C. A. (2011) Cubbing in proapolipoprotein maturation. *J. Lipid Res.* **52,** 1861–1864
42. Chau, P., Nakamura, Y., Fielding, C. J., and Fielding, P. E. (2006) Mechanism of preβ-HDL formation and activation. *Biochemistry* **45,** 3981–3987
43. Heinzel, K., and Bleul, C. C. (2007) The Foxn1-dependent transcripts PCOLCE2 and mPPP1R16B are not required for normal thymopoiesis. *Eur. J. Immunol.* **37,** 2562–2571
44. Francone, O. L., Ishida, B. Y., de la Llera-Moya, M., Royer, L., Happe, C., Zhu, J., Chalkey, R. J., Schaefer, P., Cox, C., Burlingame, A., Kane, J. P., and Rothblat, G. H. (2011) Disruption of the murine procollagen C-proteinase enhancer 2 gene causes accumulation of pro-apoA-I and increased HDL levels. *J. Lipid Res.* **52,** 1974–1983
45. Miles, R. R., Perry, W., Haas, J. V., Mosior, M. K., N'Cho, M., Wang, J. W., Yu, P., Calley, J., Yue, Y., Carter, Q., Han, B., Foxworthy, P., Kowala, M. C., Ryan, T. P., Solenberg, P. J., and Michael, L. F. (2013) Genome-wide screen for modulation of hepatic apolipoprotein A-I (ApoA-I) secretion. *J. Biol. Chem.* **288,** 6386–6396
46. Zabalawi, M., Bhat, S., Loughlin, T., Thomas, M. J., Alexander, E., Cline, M., Bullock, B., Willingham, M., and Sorci-Thomas, M. G. (2003) Induction of fatal inflammation in LDL receptor and ApoA-I double-knockout mice fed dietary fat and cholesterol. *Am. J. Pathol.* **163,** 1201–1213
47. Wilhelm, A. J., Zabalawi, M., Grayson, J. M., Weant, A. E., Major, A. S., Owen, J., Bharadwaj, M., Walzem, R., Chan, L., Oka, K., Thomas, M. J., and Sorci-Thomas, M. G. (2009) Apolipoprotein A-I and its role in lymphocyte cholesterol homeostasis and autoimmunity. *Arterioscler. Thromb. Vasc. Biol.* **29,** 843–849
48. Potteaux, S., Gautier, E. L., Hutchison, S. B., van Rooijen, N., Rader, D. J., Thomas, M. J., Sorci-Thomas, M. G., and Randolph, G. J. (2011) Suppressed monocyte recruitment drives macrophage removal from atherosclerotic plaques of Apoe$^{-/-}$ mice during disease regression. *J. Clin. Invest.* **121,** 2025–2036
49. Sorci-Thomas, M. G., Zabalawi, M., Bharadwaj, M. S., Wilhelm, A. J., Owen, J. S., Asztalos, B. F., Bhat, S., and Thomas, M. J. (2012) Dysfunctional HDL containing L159R ApoA-I leads to exacerbation of atherosclerosis in hyperlipidemic mice. *Biochim. Biophys. Acta* **1821,** 502–512
50. Bhat, S., Sorci-Thomas, M. G., Alexander, E. T., Samuel, M. P., and Thomas, M. J. (2005) Intermolecular contact between globular N-terminal fold and C-terminal domain of ApoA-I stabilizes its lipid-bound conformation: studies employing chemical cross-linking and mass spectrometry. *J. Biol. Chem.* **280,** 33015–33025
51. Bhat, S., Sorci-Thomas, M. G., Tuladhar, R., Samuel, M. P., and Thomas, M. J. (2007) Conformational adaptation of apolipoprotein A-I to discretely sized phospholipid complexes. *Biochemistry* **46,** 7811–7821
52. Bhat, S., Sorci-Thomas, M. G., Calabresi, L., Samuel, M. P., and Thomas, M. J. (2010) Conformation of dimeric apolipoprotein A-I Milano on recombinant lipoprotein particles. *Biochemistry* **49,** 5213–5224
53. Sorci-Thomas, M. G., Parks, J. S., Kearns, M. W., Pate, G. N., Zhang, C., and Thomas, M. J. (1996) High level secretion of wild-type and mutant forms of human proapoA-I using baculovirus-mediated Sf-9 cell expression. *J. Lipid Res.* **37,** 673–683
54. Kaluzny, M. A., Duncan, L. A., Merritt, M. V., and Epps, D. E. (1985) Rapid separation of lipid classes in high yield and purity using bonded phase columns. *J. Lipid Res.* **26,** 135–140
55. Schwenke, D. C., Rudel, L. L., Sorci-Thomas, M. G., and Thomas, M. J. (2002) α-Tocopherol protects against diet induced atherosclerosis in New Zealand white rabbits. *J. Lipid Res.* **43,** 1927–1938
56. Berquin, I. M., Min, Y., Wu, R., Wu, J., Perry, D., Cline, J. M., Thomas, M. J., Thornburg, T., Kulik, G., Smith, A., Edwards, I. J., D'Agostino, R., Zhang, H., Wu, H., Kang, J. X., and Chen, Y. Q. (2007) Modulation of

prostate cancer genetic risk by omega-3 and omega-6 fatty acids. *J. Clin. Invest.* **117,** 1866–1875
57. McFarlane, A. (1958) Efficient trace-labelling of proteins with iodine. *Nature* **182,** 53
58. Sorci-Thomas, M. G., Thomas, M., Curtiss, L., and Landrum, M. (2000) Single repeat deletion in ApoA-I blocks cholesterol esterification and results in rapid catabolism of delta6 and wild-type ApoA-I in transgenic mice. *J. Biol. Chem.* **275,** 12156–12163
59. Huggins, K. W., Colvin, P. L., Burleson, E. R., Kelley, K., Sawyer, J. K., Barrett, P. H., Rudel, L. L., and Parks, J. S. (2001) Dietary n-3 polyunsaturated fat increases the fractional catabolic rate of medium-sized HDL particles in African green monkeys. *J. Lipid Res.* **42,** 1457–1466
60. Junqueira, L. C., Bignolas, G., and Brentani, R. R. (1979) Picrosirius staining plus polarization microscopy, a specific method for collagen detection in tissue sections. *Histochem. J.* **11,** 447–455
61. Zhang, Y., Zanotti, I., Reilly, M. P., Glick, J. M., Rothblat, G. H., and Rader, D. J. (2003) Overexpression of apolipoprotein A-I promotes reverse transport of cholesterol from macrophages to feces *in vivo*. *Circulation* **108,** 661–663
62. Alexander, E. T., Vedhachalam, C., Sankaranarayanan, S., de la Llera-Moya, M., Rothblat, G. H., Rader, D. J., and Phillips, M. C. (2014) Influence of apolipoprotein A-I domain structure on macrophage reverse cholesterol transport in mice. *Arterioscler. Thromb. Vasc. Biol.* **31,** 320–327
63. Batta, A. K., Salen, G., Rapole, K. R., Batta, M., Batta, P., Alberts, D., and Earnest, D. (1999) Highly simplified method for gas-liquid chromatographic quantitation of bile acids and sterols in human stool. *J. Lipid Res.* **40,** 1148–1154
64. Connelly, M. A., Klein, S. M., Azhar, S., Abumrad, N. A., and Williams, D. L. (1999) Comparison of class B scavenger receptors, CD36 and scavenger receptor BI (SR-BI), shows that both receptors mediate high density lipoprotein-cholesteryl ester selective uptake but SR-BI exhibits a unique enhancement of cholesteryl ester uptake. *J. Biol. Chem.* **274,** 41–47
65. Lowry, O. H., Rosebrough, N. J., Farr, A. L., and Randall, R. J. (1951) Protein measurement with the Folin phenol reagent. *J. Biol. Chem.* **193,** 265–275
66. Wilhelm, A. J., Zabalawi, M., Owen, J. S., Shah, D., Grayson, J. M., Major, A. S., Bhat, S., Gibbs, D. P., Jr., Thomas, M. J., and Sorci-Thomas, M. G. (2010) Apolipoprotein A-I modulates regulatory T cells in autoimmune LDLr$^{-/-}$, ApoA-I$^{-/-}$ mice. *J. Biol. Chem.* **285,** 36158–36169
67. Zabalawi, M., Bharadwaj, M., Horton, H., Cline, M., Willingham, M., Thomas, M. J., and Sorci-Thomas, M. G. (2007) Inflammation and skin cholesterol in LDLr$^{-/-}$, ApoA-I$^{-/-}$ mice: link between cholesterol homeostasis and self-tolerance? *J. Lipid Res.* **48,** 52–65
68. Goldsmith, E. C., Bradshaw, A. D., and Spinale, F. G. (2013) Cellular mechanisms of tissue fibrosis. 2. Contributory pathways leading to myocardial fibrosis: moving beyond collagen expression. *Am. J. Physiol. Cell Physiol.* **304,** C393–C402
69. Canty, E. G., and Kadler, K. E. (2005) Procollagen trafficking, processing and fibrillogenesis. *J. Cell Sci.* **118,** 1341–1353
70. Baicu, C. F., Zhang, Y., Van Laer, A. O., Renaud, L., Zile, M. R., and Bradshaw, A. D. (2012) Effects of the absence of procollagen C-endopeptidase enhancer-2 on myocardial collagen accumulation in chronic pressure overload. *Am. J. Physiol. Heart Circ. Physiol.* **303,** H234–H240
71. Moali, C., Font, B., Ruggiero, F., Eichenberger, D., Rousselle, P., François, V., Oldberg, A., Bruckner-Tuderman, L., and Hulmes, D. J. (2005) Substrate-specific modulation of a multisubstrate proteinase: C-terminal processing of fibrillar procollagens is the only BMP-1-dependent activity to be enhanced by PCPE-1. *J. Biol. Chem.* **280,** 24188–24194
72. Ricard-Blum, S., Bernocco, S., Font, B., Moali, C., Eichenberger, D., Farjanel, J., Burchardt, E. R., van der Rest, M., Kessler, E., and Hulmes, D. J. (2002) Interaction properties of the procollagen C-proteinase enhancer protein shed light on the mechanism of stimulation of BMP-1. *J. Biol. Chem.* **277,** 33864–33869
73. Puppione, D. L., Yam, L. M., Bassilian, S., Souda, P., Castellani, L. W., Schumaker, V. N., and Whitelegge, J. P. (2006) Mass spectral analysis of the apolipoproteins on mouse high density lipoproteins: detection of post-translational modifications. *Biochim. Biophys. Acta* **1764,** 1363–1371
74. Zhang, Y., Da Silva, J. R., Reilly, M., Billheimer, J. T., Rothblat, G. H., and Rader, D. J. (2005) Hepatic expression of scavenger receptor class B type I (SR-BI) is a positive regulator of macrophage reverse cholesterol transport *in vivo*. *J. Clin. Invest.* **115,** 2870–2874
75. Tsukamoto, K., Buck, L., Inman, W., Griffith, L., Kocher, O., and Krieger, M. (2013) Challenges in using cultured primary rodent hepatocytes or cell lines to study hepatic HDL receptor SR-BI regulation by its cytoplasmic adaptor PDZK1. *PLoS One* **8,** e69725
76. Harder, C. J., Vassiliou, G., McBride, H. M., and McPherson, R. (2006) Hepatic SR-BI-mediated cholesteryl ester selective uptake occurs with unaltered efficiency in the absence of cellular energy. *J. Lipid Res.* **47,** 492–503
77. Tavori, H., Su, Y. R., Yancey, P. G., Giunzioni, I., Wilhelm, A. J., Blakemore, J. L., Zabalawi, M., Linton, M. F., Sorci-Thomas, M. G., and Fazio, S. (2015) Macrophage apoAI protects against dyslipidemia-induced dermatitis and atherosclerosis without affecting HDL. *J. Lipid Res.* **56,** 635–643
78. Krieger, M., and Kozarsky, K. (1999) Influence of the HDL receptor SR-BI on atherosclerosis. *Curr. Opin. Lipidol.* **10,** 491–497
79. Vergeer, M., Holleboom, A. G., Kastelein, J. J., and Kuivenhoven, J. A. (2010) The HDL hypothesis: does high-density lipoprotein protect from atherosclerosis? *J. Lipid Res.* **51,** 2058–2073
80. West, M., Greason, E., Kolmakova, A., Jahangiri, A., Asztalos, B., Pollin, T. I., and Rodriguez, A. (2009) Scavenger receptor class B type I protein as an independent predictor of high-density lipoprotein cholesterol levels in subjects with hyperalphalipoproteinemia. *J. Clin. Endocrinol. Metab.* **94,** 1451–1457
81. Chadwick, A. C., and Sahoo, D. (2012) Functional characterization of newly-discovered mutations in human SR-BI. *PLoS One* **7,** e45660
82. Chadwick, A. C., and Sahoo, D. (2013) Functional genomics of the human high-density lipoprotein receptor scavenger receptor BI: an old dog with new tricks. *Curr. Opin. Endocrinol. Diabetes Obes.* **20,** 124–131
83. Reaven, E., Cortez, Y., Leers-Sucheta, S., Nomoto, A., and Azhar, S. (2004) Dimerization of the scavenger receptor class B type I: formation, function, and localization in diverse cells and tissues. *J. Lipid Res.* **45,** 513–528
84. Sahoo, D., Darlington, Y. F., Pop, D., Williams, D. L., and Connelly, M. A. (2007) Scavenger receptor class B type I (SR-BI) assembles into detergent-sensitive dimers and tetramers. *Biochim. Biophys. Acta* **1771,** 807–817
85. Sahoo, D., Peng, Y., Smith, J. R., Darlington, Y. F., and Connelly, M. A. (2007) Scavenger receptor class B, type I (SR-BI) homo-dimerizes via its C-terminal region: fluorescence resonance energy transfer analysis. *Biochim. Biophys. Acta* **1771,** 818–829
86. Kartz, G. A., Holme, R. L., Nicholson, K., and Sahoo, D. (2014) SR-BI/CD36 chimeric receptors define extracellular subdomains of SR-BI critical for cholesterol transport. *Biochemistry* **53,** 6173–6182
87. Kocher, O., and Krieger, M. (2009) Role of the adaptor protein PDZK1 in controlling the HDL receptor SR-BI. *Curr. Opin. Lipidol.* **20,** 236–241
88. Saddar, S., Mineo, C., and Shaul, P. W. (2010) Signaling by the high-affinity HDL receptor scavenger receptor B type I. *Arterioscler. Thromb. Vasc. Biol.* **30,** 144–150
89. Pittman, R. C., Knecht, T. P., Rosenbaum, M. S., and Taylor, C. A., Jr. (1987) A nonendocytotic mechanism for the selective uptake of high density lipoprotein-associated cholesterol esters. *J. Biol. Chem.* **262,** 2443–2450
90. Silver, D. L., Wang, N., Xiao, X., and Tall, A. R. (2001) High density lipoprotein (HDL) particle uptake mediated by scavenger receptor class B type 1 results in selective sorting of HDL cholesterol from protein and polarized cholesterol secretion. *J. Biol. Chem.* **276,** 25287–25293
91. Pagler, T. A., Rhode, S., Neuhofer, A., Laggner, H., Strobl, W., Hinterndorfer, C., Volf, I., Pavelka, M., Eckhardt, E. R., van der Westhuyzen, D. R., Schütz, G. J., and Stangl, H. (2006) SR-BI-mediated high density lipoprotein (HDL) endocytosis leads to HDL resecretion facilitating cholesterol efflux. *J. Biol. Chem.* **281,** 11193–11204
92. Röhrl, C., and Stangl, H. (2013) HDL endocytosis and resecretion. *Biochim. Biophys. Acta* **1831,** 1626–1633

Procollagen C-endopeptidase Enhancer Protein 2 (PCPE2) Reduces Atherosclerosis in Mice by Enhancing Scavenger Receptor Class B1 (SR-BI)-mediated High-density Lipoprotein (HDL)-Cholesteryl Ester Uptake

Ricquita D. Pollard, Christopher N. Blesso, Manal Zabalawi, Brian Fulp, Mark Gerelus, Xuewei Zhu, Erica W. Lyons, Nebil Nuradin, Omar L. Francone, Xiang-An Li, Daisy Sahoo, Michael J. Thomas and Mary G. Sorci-Thomas

J. Biol. Chem. 2015, 290:15496-15511.
doi: 10.1074/jbc.M115.646240 originally published online May 6, 2015
